Zika virus induces mitotic catastrophe in human neural progenitors by triggering unscheduled mitotic entry in the presence of DNA damage while functionally depleting nuclear PNKP.

Malgorzata Rychlowska[1], Abigail Agyapong[1], Michael Weinfeld[2], Luis M. Schang[1*]

*corresponding author

[1] Baker Institute for Animal Health and Department of Microbiology and Immunology, College of Veterinary Medicine, Cornell University, USA

[2] Department of Oncology, Division of Experimental Oncology, University of Alberta, Canada

Email

MR: mr783@cornell.edu

AA: aa845@cornell.edu

MW: mweinfel@ualberta.ca

LMS: luis.schang@cornell.edu

Keywords

ZIKV; congenital Zika virus syndrome; microcephaly; mitotic catastrophe; unscheduled mitotic entry; cyclin dependent kinase 1; CDK1; DNA damage repair; polynucleotide kinase 3'-phosphatase; PNKP; microcephaly, seizures, and developmental delay; MCSZ

Abstract

Vertical transmission of Zika virus (ZIKV) leads with high frequency to congenital ZIKV syndrome (CZS), whose worse outcome is microcephaly. However, the mechanisms of congenital ZIKV neurodevelopmental pathologies, including direct cytotoxicity to neural progenitor cells (NPC), placental insufficiency, and immune responses, remain incompletely understood. At the cellular level, microcephaly typically results from death or insufficient proliferation of NPC or cortical neurons. NPCs replicate fast, requiring efficient DNA damage responses to ensure genome stability. Like congenital ZIKV infection, mutations in the polynucleotide 5'-kinase 3'-phosphatase (PNKP) gene, which encodes a critical DNA damage repair enzyme, results in recessive syndromes often characterized by congenital microcephaly with seizures (MCSZ). We thus tested whether there were any links between ZIKV and PNKP.

Here we show that a PNKP phosphatase inhibitor inhibits ZIKV replication. PNKP relocalized from the nucleus to the cytoplasm in infected cells, co-localizing with the marker of ZIKV replication factories (RF) NS1 and resulting in functional nuclear PNKP depletion. Although infected NPC accumulated DNA damage, they failed to activate the DNA damage checkpoint kinases Chk1 and Chk2. ZIKV also induced activation of

cytoplasmic CycA/CDK1 complexes, which trigger unscheduled mitotic entry. Inhibition of CDK1 activity inhibited ZIKV replication and the formation of RF, supporting a role of cytoplasmic CycA/CDK1 in RF morphogenesis. In brief, ZIKV infection induces mitotic catastrophe resulting from unscheduled mitotic entry in the presence of DNA damage. PNKP and CycA/CDK1 are thus host factors participating in ZIKV replication in NPC, and probably pathogenesis.

Significance

The 2015-2017 Zika virus (ZIKV) outbreak in Brazil and subsequent international epidemic revealed the strong association between ZIKV infection and congenital malformations, mostly neurodevelopmental defects up to microcephaly. The scale and global expansion of the epidemic, the new ZIKV outbreaks (Kerala state, India, 2021), and the potential burden of future ones pose a serious ongoing risk. However, the cellular and molecular mechanisms resulting in microcephaly remain incompletely understood. Here we show that ZIKV infection of neuronal progenitor cells results in cytoplasmic sequestration of an essential DNA repair protein itself associated with microcephaly, with the consequent accumulation of DNA damage, together with an unscheduled activation of cytoplasmic CDK1/Cyclin A complexes in the presence of DNA damage. These alterations result in mitotic catastrophe of neuronal progenitors, which would lead to a depletion of cortical neurons during development.

Introduction

Since its identification in 1947, Zika virus (ZIKV) had been associated with mostly mild and asymptomatic infections until the recent international epidemic with 245,000 confirmed, and 820,000 suspected, cases (1). It took 62 years from the first documented human infection in 1954 (2) to this international epidemic in 2015-2018 to evidence the association of ZIKV infection with the congenital neurodevelopmental pathologies currently referred to as a congenital ZIKV syndrome (CZS) (3). The most significant burden of CZS is congenital microcephaly. Infants born with microcephaly have a range of health problems and suffer lifetime consequences (4, 5). Despite the global health burden, relatively little is yet known about the mechanisms of ZIKV-induced microcephaly.

ZIKV is a unique vector-born flavivirus in that it has two additional routes of transmission, sexual (6-8) and vertical (9-13). The risk of vertical transmission is as high as 46% in the 1st trimester of pregnancy, and vertically transmitted ZIKV can infect the developing fetal brain producing CZS in about 9% of babies born to mothers infected in the 1st trimester (14). Neither the mechanism of vertical or sexual transmission, nor the tropism for the developing fetal brain or the microcephaly mechanisms are fully understood. The fetal neurotoxicity of ZIKV is likely the result of a combination of multiple factors, including placental insufficiency and inflammatory responses, activation of innate immunity, and direct ZIKV induced cytotoxicity to neural progenitor cells (for recent reviews see (15, 16)). At the cellular level, congenital microcephaly is caused by the depletion of the neural progenitor cells (NPC), which are responsible for brain development, either by cell death or premature differentiation (17). Proliferating NPC are the primary target for ZIKV, as

demonstrated in human autopsies, animal models, and in vitro cell culture systems. ZIKV infection of NPC leads to reduced proliferation and cell death (reviewed in refs. (16, 18)).

Zika virus (ZIKV) is a mosquito-born RNA virus in the *Flavivirus* genus of the *Flaviviridae* family, which comprises several other important arthropod-born human pathogens like dengue virus (DENV), yellow fever virus (YFV), West Nile virus (WNV), and Japanese encephalitis virus (JEV). Like all viruses in this family, ZIKV has a single stranded, positive sense RNA (ss(+)RNA) genome encoding a single ORF, which is directly translated into a precursor polyprotein (19). The polyprotein is then proteolytically cleaved into the individual viral proteins, including the structural proteins, capsid, E and prM/M, which are incorporated into viral particles, and the non-structural (NS) proteins, NS1, NS2A, NS2B, NS3, NS4A, NS4B and NS5, which are expressed in the infected cell and responsible for viral replication and assembly (20, 21).

Like all ss(+)RNA viruses, ZIKV has a cytoplasmic replication cycle and remodels the endoplasmic reticulum (ER) membranes to assemble the viral replication factories (RF) (22). The characteristic ER rearrangements in Flavivirus infections take the shape of dilated ER cisternae containing numerous invaginated vesicles (Ve), vesicular packets (Vp), tubular network of convoluted membranes (CM), and zippered ER (zER) (22-26). These RF enable the concentration of the viral factors required for replication and assembly of progeny virions. Invaginated towards the ER lumen with a narrow opening to the cytoplasm, the Ve contain fully assembled viral replication complexes (RC). Such a semi-open structure is crucial for recruiting the cytoplasmic viral enzymes NS3 (protease and helicase) and NS5 (methyltransferase and RNA-dependent RNA

polymerase), while at the same time shielding the viral genomes from recognition and degradation (22, 27). The formation of RF is thus essential for the viral replication cycle.

Several cellular and viral factors play important roles in the biogenesis of RF (for a recent review see ref. (28)). One of them is the viral non-structural protein 1 (NS1), which localizes to the ER lumen and binds to the inner leaflet of the ER membrane via hydrophobic interactions. Free luminal NS1 also enters the secretory pathway and is secreted (29, 30). Membrane binding and dimerization or multimerization of NS1 induces membrane curvature leading to the formation of invaginations directed towards the ER lumen, thus initiating the shaping of the Ve (25). There is also mounting evidence that flaviviral NS2A, 2B, 4A and 4B, as well as several cellular proteins, play important roles in the biogenesis of RF (28). The formation and maintenance of ZIKV RFs is thus a combined effort of several NS and cellular proteins.

ZIKV is only a minor cause of global microcephaly, with over 3,720 confirmed CZS cases worldwide (1). The vast majority of microcephalies with identified etiology result from genetic disorders, including mutations in one of the essential DNA damage repair proteins, polynucleotide kinase 3'-phosphatase (PNKP). These mutations are associated with a primary form of microcephaly, named microcephaly, seizures, and developmental delay (MCSZ) (31-33).

PNKP is a DNA processing enzyme that restores canonical termini at DNA breaks through its 5' DNA kinase and 3'-phosphatase activities (34-36). Some DNA breaks have noncanonical 3'-phosphate (3'-PO) or 5'-hydroxyl (5'-OH) groups, which cannot be processed by cellular DNA ligases or polymerases. Reactive oxygen species (ROS) produce predominantly DNA breaks harboring 3'-phosphate termini (37), which are also

common in DNA breaks induced by ionizing irradiation, stalled topoisomerase I (TOP1) complexes, and as intermediate products of base excision DNA repair (BER). 5'-OH termini are also common products of ionizing radiation or abortive TOP1 reactions (38-42). Although chromatin organization protects DNA from mechanical stresses, its condensation at repairing or replicating DNA sites induces sufficient mechanical stresses to result in DNA breaks (43). Therefore, physical forces are another important mechanism producing DNA breaks which need not have canonical termini. Both 5'-OH and 3'-PO DNA ends are substrates for PNKP.

PNKP deficiencies cause the expected accumulation of DNA breaks, affecting particularly neural progenitor cells, and thus leading to neurodevelopmental and neurodegenerative disorders (44-47). Experimental PNKP depletion causes embryonic death or congenital microcephaly in animal models, depending on the residual levels of enzymatic activities (44, 47). Targeted PNKP deletion restricted to the nervous system resulted in early postnatal lethality in a mouse model. Massive cell death occurred through many still proliferating regions of the developing nervous system. This cell death produced neurodevelopmental defects leading to thinning or even complete loss of the neural cortex (47).

DNA damage is detrimental to genome stability. Therefore, DNA damage signaling activates DNA damage checkpoints to stop cell cycle progression and allow for DNA repair before proceeding into genome replication (DNA synthesis, S phase) or cell division (mitosis, M phase). Cell-cycle progression is driven by the periodical activation and inactivation of the cyclin-dependent kinases (CDKs). Activation of CDK1 determines the commitment of a cell to mitosis, whereas its inactivation promotes mitotic exit. Scheduled

activation and inactivation of CDK1 are thus essential for successful mitosis and progression through the cell cycle (for a comprehensive review see ref. (48)). CDK activity is regulated by regulatory subunits, the cyclins, post-translational modifications, association with other proteins, and subcellular localization. In brief, CDK activation requires binding to their regulatory cyclins, phosphorylation at the activation loop, removal of other inhibitory phosphates, and no inhibition by the CIP/KIP or INK4 CDK inhibitors (48).

Unscheduled mitotic entry in the presence of DNA damage is rare, and it occurs primarily in response to chemo- or radiotherapy in cancer cells defective in checkpoint signaling. Under these conditions, cells undergo catastrophic mitoses producing abnormal nuclear morphologies due to defective chromosome segregation (for a comprehensive review see ref. (49))

To prevent mitotic catastrophe, mutagenesis, and other cytopathologies, mitotic entry is highly regulated. It is initiated by the threshold activation of CDK1 (for a recent review see ref. (50)), which is primarily limited by cyclin availability. CDK1 associates with two types of mitotic cyclins, A or B, which are expressed and degraded in a highly regulated fashion. Cyclin A (CycA) starts to accumulate in S phase and first associates with CDK2, with CycA/CDK activity starting to be detected in early S phase (51). Cyclin B (CycB) starts to accumulate in G2, with CycB/CDK1 activity first detected at mitosis. Both CycA and CycB are degraded in mitosis by regulated ubiquitination-proteasome system. CycA levels decline rapidly after the nuclear envelope breakdown, with degradation completed at prometaphase (52, 53). CycB degradation is initiated by the activated anaphase promoting complex/cyclosome (APC/C) at metaphase. Both CycA and B are thus

degraded at the onset of anaphase, rendering CDK1 inactive (reviewed in ref. (54, 55)), and this inactivation is required for mitotic exit. The activity of Cyclin/CDK1 is additionally controlled by inhibitory CDK1 phosphorylations at Thr14 (56-58) and Tyr15 (56, 59) and the activating phosphorylation at Thr161 (60, 61). Phosphorylation on Tyr15, in particular, prevents unscheduled mitotic entry by keeping CycA or B/CDK1 complexes inactive. The CDC25 family phosphatases activate CycB/CDK1 at the onset of mitosis by removing these inhibitory phosphate groups (62-64). Activation of the DNA damage checkpoints inactivates CDC25 phosphatases, thus preventing CDK1 activation and delaying mitotic entry until the DNA damage signaling is turned off.

Both ZIKV and PNKP deficiencies specifically affect human neural progenitor cells, leading to their massive loss during fetal development. Both induce DNA damage and produce chromosomal abnormalities leading to abnormal mitoses. We thus explored whether PNKP could be a cellular factor for ZIKV replication in human iPSC-derived neural progenitor cells (hiNPC) and other cells. We explored potential molecular mechanisms for the direct cytotoxicity of ZIKV to human neural progenitor cells by testing the effects of PNKP inhibition on ZIKV replication and the influence of ZIKV infection on PNKP, the DNA damage operated cell cycle checkpoints, and mitotic entry.

Materials and methods

Cell lines. African green monkey Vero E76, human U-2 OS osteosarcoma and HEK-293 embryonic kidney cells were obtained from American Tissue Culture Collection (CCL-81, HTB-96, CRL-1573, respectively). Cells were cultured in DMEM supplemented with 5% FBS at 37°C in 5% CO_2. Human induced pluripotent stem cell-derived neural progenitor

cells (HIP Neural Stem Cells, BC1 line, referred to as 'hiNPC') were purchased form MTI-GlobalStem, Inc. (GSC-4311). Cells were grown as monolayers on geltrex-coated surfaces (Geltrex™ LDEV-Free reduced growth factor basement membrane matrix, Gibco, A1413201) in NPC expansion medium: KnockOut™ DMEM/F-12 (Gibco, 12660012) supplemented with StemPro™ neural supplement (Gibco, A1050801), 2 mM (1X) Glutagro (L- Alanine/L-Glutamine dipeptide, Corning), 1X MEM non-essential amino acids (Corning), and 20 ng/mL human heat stable sbFGF (Gibco, PHG0367) and split using accutase (Millipore Sigma, A6964).

Compounds and treatments. The PNKP inhibitor A12B4C3 was synthesized as previously reported (65, 66) and kindly provided by Dr. Dennis Hall (University of Alberta). DMSO stocks of A12B4C3 (10 mM) were prepared in dimethyl sulfoxide (DMSO), aliquoted and stored at -20°C. Frozen aliquots were thawed fast at 37°C and diluted to target concentrations (20-0.01 μM) in tissue culture media. Roscovitine (Rosco, LC Laboratories, R-1234) stock solution was prepared at 100 mM in DMSO aliquoted and stored at -20°C. Frozen aliquots were thawed fast at 37°C and diluted to 100-0.1 μM in pre-warmed DMEM-5% FBS. Compounds were added to cells after removing the inocula and washing with serum free media. Hydrogen peroxide (H_2O_2), and ultraviolet irradiation (UV) were used to induce DNA damage. Working solution of 100 μM H_2O_2 was prepared by diluting 30% stock solution in serum-free culture media immediately before adding to cells. After 60 min incubation at 37°C in 5% CO_2, the H_2O_2 containing medium was aspirated and cells were washed twice in serum free medium. Complete media (DMEM + 5%FBS or NPC expansion medium) was then added, and cells were returned to the incubator for 1 h. Alternatively cells were washed and overlaid with phenol red free-

DMEM, irradiated with UV at 100 J/m^2 (Spectrolinker XL-1000 UV crosslinker. Spectronics Corp.) and allowed to recover for 1 h in the complete culture medium. Cells were subsequently fixed and processed by immunostaining or lysed and used for Western blotting.

Viruses. ZIKV strains R103451 (placenta isolate, Human/2015/Honduras) or IbH 30656 (blood isolate, Human/1968/Nigeria) were obtained from BEI resources (NR-50066 and NR-50355, respectively). Stocks were prepared by inoculation of sub-confluent monolayers of U-2 OS cells seeded in T150 flask 24 h earlier at an moi of 0.001 in 2 ml DMEM for 1 h. Inoculum was removed and cells were washed twice with 12 ml cold DMEM before overlaying with 15 ml DMEM-5% FBS. Infected cells were incubated for 24 h at 37°C in 5% CO_2 to reach confluence, and then split 1:3. Supernatants were harvested 5 days post inoculation and cells were overlaid with 15 ml DMEM-5%FBS. Typically, 3-4 harvests were collected every 4-5 days before cells reached full cytopathic effect. Collected medium was clarified by centrifugation at 3,000 g for 10 minutes at 4°C. Cleared culture media was concentrated 10 times for each harvest, using 50 mL 100K Amicon Ultra centrifugation tubes spun at 3500 g for 25 minutes at 4°C. Retentates were aliquoted into 500 μL, frozen in ethanol-dry ice bath and stored at -80°C.

Antibodies. Primary and secondary antibodies are listed in Supplementary Tables 1 and 2 (**Suppl. Tab.1, 2**)

ZIKV infections. For immunofluorescence (IF), $3x10^5$ (hiNPC) or $1.5x10^5$ (U-2 OS, Vero, 293) cells were seeded onto geltrex-coated (hiNPC) or uncoated (U-2 OS, Vero, HEK-293) 21 mm diameter round coverslips in 12-well plates and infected 24 h later with 1-3 foci forming units (FFU) (hiNPC) or 1-3 plaque forming units (PFU) (other cells) per cell

of ZIKV in 150 ml of expansion medium (hiNPC) or DMEM (other cells). Inoculated cells were incubated for 1 h at 37°C, rocking and rotating every 10-15 min. Cells were washed once with 2 ml/well cold KnockOut DMEM:F12 (hiNPC) or DMEM (other cells) before overlaying with 1.5 ml/well 37°C complete expansion medium (hiNPC) or DMEM-5% FBS (other cells) and incubated at 37°C in 5% CO_2. Cells were fixed and processed by immunostaining at pre-selected times.

For drug treatments, cells were seeded on geltrex-coated 12-well plates as described and infected 24 h later with 3 FFU (hiNPC) or 3 PFU (other cells) per cell of ZIKV as described. Culture media were harvested at pre-selected times, cleared by centrifugation at 3,000 g for 10 minutes at 4°C, and titrated immediately or frozen at -80°C for later titration.

For Western blotting or immuno-kinase activity assays, $3x10^6$ cells were seeded on T75 flasks or 10 cm diameter dishes and infected 24 h later with 3 FFU (hiNPC) or 3 PFU (U-2 OS) per cell of ZIKV in 1 ml serum free medium, as described. Cell monolayers were detached with accutase (hiNPC), or trypsin (U-2 OS) at pre-selected times, pelleted, resuspended in 1 ml ice-cold PBS (10 μl aliquots were used for cell counting) and pelleted again. PBS was aspirated and cell pellets were frozen at -80°C until further processing.

Plaque forming assays. Vero cells ($1.2x\ 10^5$) were seeded into each well of 12-well plates and incubated at 37°C in 5% CO_2. Cells were inoculated with 150 μl of sample the following day and incubated for 1 h at 37°C, rocking and rotating every 10 min. Cells were washed twice with 2 ml/well cold DMEM before overlaying with 1.5 ml/well 37°C DMEM-5% FBS containing 1% methylcellulose and incubating at 37°C in 5% CO_2 until plaques developed, typically 4-6 days. Cells were fixed and stained overnight with 0.5% crystal violet in 17% methanol. Plaque numbers are expressed as PFU/ml for titration of viral

stocks or normalized to infected cell number and expressed as PFU/cell (virus burst) for dose response or time of addition analyses.

Foci formation assays. ZIKV infectious titers in hiNPC we evaluated by FFU. hiNPC (3.0 x 10^5 cells/well) were seeded into Geltrex-coted 12-well plates in 1 ml of NPC expansion medium, and incubated at 37°C in 5% CO2. Cells were inoculated 24 h later with 150 µl per well of serial dilutions of ZIKV stocks in the expansion medium and incubated at 37°C for 1 h, rocking and rotating every 10-15 min. Inocula were removed and cells were washed twice with 1.5 ml/well cold unsuplemented KnockOut DMEM:F12. Cells were overlaid with 1 ml/well expansion medium, containing 0.75% methylcellulose and incubated for 48 h at 37°C and 5% CO2. Cells were fixed and processed for indirect immunofluorescence for flavivirus group E antigen (clone 4G2). Calculated foci numbers were expressed as FFU/ml.

Time of addition assay. hiNPC cells were infected with 3 FFU of ZIKV/cell. After 1 h adsorption, cells were washed and overlaid with 2 ml drug-free expansion medium or expansion medium containing 100 µM Rosco. Drug-free expansion medium was removed at 3, 6, 9, 12, or 15 hpi from replicate series of infected monolayers and replaced with 2 ml of expansion medium containing 100 µM Rosco. An additional series of infected monolayers was incubated continuously in vehicle (0.1% DMSO) containing drug-free expansion medium. For each time of addition, culture media were sampled just before Rosco addition and at the end of experiment (24 hpi), to calculate viral burst from the time of drug addition. To this end, 100 µl of medium was removed and substituted with 100 µl fresh expansion media. Samples were frozen at -80ºC until titrated on Vero cells. For untreated infections, culture medium was equally sampled at every time-point from 1 to

15 h, and then at 24 h. Viral burst, as percent of burst in vehicle control, is plotted against hours post infection (hpi). Each time point indicates the average and range of two independent experiments.

Immuno complex kinase assay. Cell lysates were prepared by resuspending cell pellets to $1x10^4$ cells/μl in non-denaturing lysis buffer (50 mM Tris-HCl, pH7.4, 1 mM EDTA, 1 mM EGTA, 150 mM NaCl, 1% Triton X-100), supplemented with protease and phosphatase inhibitor cocktails (cOmplete, EDTA-free and PhosSTOP from Roche) and incubated for 30 min at 4°C. Lysates were cleared by centrifugation (15,000 xg, 15 min, 4°C) before 100 μl of supernatant, equivalent to $1x10^6$ cells, was incubated with 25 μl of agarose-coupled anti-CDK1 or anti-CycA2 antibodies (sc-54AC or sc-239AC, Santa Cruz Biotechnology, respectively) for 2 h at 4 °C with gentle rocking. After three washes in lysis buffer and one wash in kinase buffer (50 mM Tris-HCl, pH 7.4, 10 mM $MgCl_2$, 1 mM DTT), kinase assays were performed by incubating the immunoprecipitated proteins and beads in 30 μl kinase buffer supplemented with 50 μM ATP and 3 μg histone H1 (EMD Millipore, 14-155) for 30 min at room temperature. Kinase activity was measured using ADP-Glo Kinase assay (V6930, Promega) according to the manufacturer's instructions. Luminescence was measured using a TECAN infinite 200Pro plate reader. Kinase activity, proportional to relative luminesce units (RLU), was plotted against time after infection.

Indirect immunofluorescence. For confocal imaging, cells were fixed with 3.7% buffered formaldehyde for 15 min at room temperature. Fixative was removed, cells were washed three times with 1 ml PBS each, permeabilized with 0.5% Triton X100 in PBS for 15 minutes at RT, and blocked with 500 µl 5% normal goat serum (NGS) in PBS for 1 h

at room temperature (RT). Primary antibodies (**Suppl. Tab. 1**) were diluted in 1% NGS in PBS and incubated overnight at 4°C. Primary antibodies were removed and cells were washed three times in 1 ml of 0.2% TritonX100 in PBS each time. Fluorescently-conjugated secondary antibodies (**Suppl. Tab. 2**) were diluted 1:1,000 in 1% NGS in PBS, incubated for 1 h at room temperature protected from light and washed 3 times in 1 ml each wash of 0.2% TritonX100 in PBS.

Cells were counterstained with 2 μg/ml DAPI in PBS for 5 min at room temperature. Coverslips were removed from the wells, rinsed briefly in dH_2O, and mounted onto glass microscope slides using 10 μl Prolong Gold (Molecular Probes, P10144) or Prolong Glass (Invitrogen, P36984) antifade mounting media. The slides were protected from light until imaging by confocal microscopy using a Zeiss LSM 510 or an Olympus FV 3000 microscopes and ZEN2.3ProHWL or FV315-SW image acquisition software, respectively. ImageJ software (67) was used to convert raw image stacks to single channel (grey scale) or merged (color scale) images and to add scale bars.

Metabolic labeling with EdU. hiNPC (2.5×10^5) were seeded on geltrex-coated 21 mm diameter glass coverslips in 1.0 ml growth medium. 24 hours after plating, 1.0 ml of 20 μM EdU in growth medium was added (10 μM final concentration) and cells were returned to the incubator for a 15 min pulse labelling. Cells were subsequently fixed and permeabilized for IF as described above, blocked with 1 ml of 3% BSA in PBS, washed and stained using Click-iT™ EdU Cell Proliferation Kit for Imaging, using Alexa Fluor™ 488 dye (Thermo Fisher Scientific, C10337), according to the manufacturer's protocol. Cells were subsequently stained for ZIKV NS1 (IF) and counterstained with DAPI.

Cytotoxicity. Cytotoxicity in hiNPC or U-2 OS cells was tested using CellTiter-Glo® luminescent cell viability assay (Promega, G7570). Cells (5 or 2.4 x 10^3 cells/well, for hiNPC or U-2 OS, respectively) were seeded in 96-well plates to reach 25% confluence at 24 h after plating. Test compound dilutions were added 24 hours later in 150 μl DMEM-5% FBS (U-2 OS) or maintenance medium (hiNPC) and incubated for 3 days at 37°C. Relative cell number was determined daily by incubating replicated monolayers with CellTiter-Glo reagent diluted in phenol-red free DMEM for 30 min at RT. Luminescence was measured using TECAN infinite 200Pro plate reader. Relative cell number was plotted against time of treatment for each drug dilution.

Western blot. Cell monolayers in T75 flasks or 10 cm diameter dishes were detached with accutase (hiNPC) or trypsin (U-2 OS), pelleted, and resuspended in 1 ml of ice-cold PBS (10 μl samples were collected for counting cells) and pelleted again. PBS was aspirated and cell pellets were frozen at -80ºC. Sufficient ice-cold lysis buffer (50 mM Tris-HCl, pH 7.4, 1 mM EDTA, 1 mM EGTA, 150 mM NaCl, 1% Triton X-100, 0.5% sodium deoxycholate, 0.5% SDS) supplemented with protease and phosphatase inhibitor cocktails (cOmplete, EDTA-free and PhosSTOP from Roche) was added to the pellets to yield 1x10^4 cell equivalent/μl. Samples were incubated for 30 min at 4ºC with rocking and then sonicated (3 x 30 sec interval, high setting in a Bioruptor water bath sonicator, Diagenode). Lysates were cleared by centrifugation at 13,000 x g for 15 min at 4°C. Supernatants were collected, mixed 4:1 with reducing NuPAGE™ LDS sample buffer 4x (ThermoFisher Scientific, NP0007) and boiled for 10 minutes. Proteins were separated by electrophoresis in 12 or 7% polyacrylamide gels (the later for high molecular weight proteins, ATM and ATR) and transferred to polyvinylidene fluoride or nitrocellulose

membranes. Membranes were blocked with TBS containing 0.1% Tween-20 (TBST) supplemented with 5% BSA. Primary antibodies (**Suppl. Tab. 1**) diluted in TBST were added and incubated overnight at 4°C with rocking. Membranes were washed with TBST three times for 10 minutes each and incubated with the corresponding fluorescently-labeled secondary antibody (**Suppl. Tab. 2**) for 1 h at room temperature with gentle rocking. Membranes were washed as described and signal was detected and recorded using a ChemiDoc MP imager (BioRad).

Results

The PNKP inhibitor A12B4C3 inhibits ZIKV replication. PNKP is an essential DNA damage repair enzyme which, like ZIKV infection, is also linked to microcephaly (31, 32). We asked whether ZIKV infection may affect, or be affected by, PNKP. To this end, we tested the effect of a PNKP inhibitor on ZIKV replication in hiNPC and human osteosarcoma U-2 OS cells. We treated already infected cells with semi-logarithmic dilutions of the PNKP inhibitor A12B4C3 and titrated the cell-free infectivity at 24 h. There was a dose response inhibition of ZIKV replication in both cell lines (EC_{50}, 3 μM) (**Fig. 1A).** A12B4C3 did not produce cytotoxic or cytostatic effects at up to 10 μM for up to 72 h in either cell line (**Suppl. Fig 1A**).

PNKP is constitutively expressed, and its levels are regulated by proteasomal degradation (68). Host factors required for viral replication are often upregulated during infection. However, PNKP levels were constant during ZIKV infection and did not differ from those in mock-infected cells **(Fig 1B, Suppl Fig. 1B**).

PNKP is cytoplasmic and co-localizes with NS1 during ZIKV infection. PNKP normally localizes to the nucleus and mitochondria (69) whereas ZIKV replicates in cytoplasmic ER-derived membranous structures (26). We thus evaluated PNKP subcellular localization in ZIKV infected cells (**Fig. 1C**). PNKP localized predominantly to the nucleus in mock infected hiNPC, showing a disperse staining pattern, as expected (69). In contrast, PNKP signal was concentrated in the cytoplasm at the center of ZIKV-infected cells, whereas abnormal and often multi-lobular nuclei occupied the cell periphery. Cytoplasmic PNKP colocalized with ZIKV non-structural protein 1 (NS1) (**Fig. 1C**).

PNKP colocalized in the cytoplasm with NS1 in about 80-95% of cells at 24 hpi (**Fig. 1D).** PNKP signal started to be depleted from the nucleus at 3 h post infection, with a gradual increase in cytoplasmic staining observed from 6 hpi. PNKP colocalization with NS1 was obvious as early as ZIKV replication factories were detected at 12 hpi, although it was detectable as soon as 9 hpi in some infected cells staining positive for NS1 (**Fig. 1E**).

Co-localization of PNKP and NS1 was not unique to neural progenitor cells. Cytoplasmic PNKP accumulation was also detected in three non-neural cell lines permissive to ZIKV replication, U-2 OS, Vero, and HEK293 (**Suppl. Fig.1C**). Notably, however, the nuclear morphology in these non-neural progenitor cells was much closer to that of their non-infected counterparts. Co-localization of PNKP with ZIKV RFs was detected using three different ZIKV-specific antibodies recognizing ZIKV NS1 or gE, or flavivirus group E antigen (**Suppl. Fig. 1C**).

PNKP relocalization was not unique to the contemporary ZIKV strain R103451 (Honduras/2016/human placenta). Cytoplasmic PNKP and abnormal nuclear morphology

were equally induced in neuronal progenitor cells by historical ZIKV strain IbH-30656 (Nigeria/1968) (**suppl. Fig. 1D**).

ZIKV-induced PNKP relocalization is independent of XRCC1 or XRCC4. PNKP is recruited to nuclear DNA damage sites by interactions with the DDR scaffold proteins XRCC1 or XRCC4 (70-72). Depending on the type of DNA damage, XRCC1 (ssDNA damage) or XRCC4 (dsDNA damage) organize multiprotein complexes at DNA lesions to concentrate DNA repair enzymes, including PNKP, DNA ligases, and polymerases, along with multiple regulatory and signaling proteins. We thus asked whether PNKP was recruited to the cytoplasm by XRCC1 or XRCC4. XRCC1 and XRCC4 are normally nuclear and both remained nuclear in ZIKV-infected hiNPC. There was no co-localization of either with NS1 (**Fig. 1F**). XRCC1 or XRCC4 therefore do not account for the cytoplasmic PNKP accumulation.

ZIKV infected hiNPC accumulate DNA damage. Downregulation or inhibition of PNKP sensitizes cells to genotoxic stress and results in accumulation of unrepaired DNA (45-47, 65, 66, 73, 74). Cytoplasmic PNKP sequestration in ZIKV infection may result in depletion of functional nuclear PNKP. Cells deficient in nuclear PNKP would then accumulate DNA damage. We used γH2AX staining to test for DNA damage. H_2O_2 treatment of uninfected cells induced the expected canonical, bright, well defined, and isolated nuclear γH2AX foci, detectable at 10 min post treatment (**Fig. 2A** and **suppl. Fig. 2A, 2B**). Infected cell nuclei strongly stained positive for γH2AX at 24 hours after infection (**Fig. 2A**). Some baseline level of γH2AX staining was detected also in mock-infected cells or at time zero after ZIKV infection, but the nuclear γH2AX foci started to obviously increase in number, size, and brightness above baseline after infection (**Suppl. Fig. 2A**),

and most ZIKV infected cells had strong nuclear γH2AX signal at 32 and 48h. Thus, ZIKV infection induces DNA damage that continues to accumulate during infection.

PNKP is not phosphorylated at the DNA damage sites in ZIKV infected cells. In response to DNA damage signaling, PNKP is recruited to the DNA breaks where it is phosphorylated by ATM. Phosphorylation allows for the accumulation of PNKP at the DNA breaks, accumulation which is necessary for efficient repair (68, 75, 76). ZIKV-induced accumulation of DNA damage could be the consequence of nonfunctional repair mechanisms due to the cytoplasmic PNKP localization (**Fig. 1C**). However, cytoplasmic PNKP could still be recruited to the nucleus, or a small population of PNKP may remain in the nucleus and be activated. We tested PNKP phosphorylation using phospho-specific PNKP antibodies (Ser114). p-PNKP accumulated in scattered nuclear foci in uninfected cells treated with H_2O_2 (**Fig. 2B,C**), as expected. Also as expected, H_2O_2-induced PNKP foci were detected at 30 min post treatment and colocalized with γH2AX foci (**Fig. 2C** and **suppl. Fig. 2B**). In contrast, there was no detectable p-PNKP signal in ZIKV infected cells, neither nuclear nor cytoplasmic (**Fig. 2B, Suppl. Fig. 2C**). No nuclear or cytoplasmic p-PNKP signal was detected at any time during ZIKV infection **(Suppl. Fig. 2C).**

ZIKV infection induces obvious gross mitotic abnormalities in hiNPC. Throughout all experiments (**Fig. 1C, E, F; 2A, B; Suppl. Fig. 2A, B**), we had been noting that ZIKV consistently induced multilobed nuclei, micronuclei, and chromosomal bridges in hiNPC, but not in other cells (**Fig. 3A, B, C**), defects which are all consistent with mitotic abnormalities. We analyzed the relative frequency of the putative mitotic aberrations in hiNPC or U-2 OS. Grossly abnormal nuclear morphologies were more frequent, and more

severe, in infected hiNPC than U-2 OS (**Fig. 3A, D**), Vero, or HEK293 cells (**Suppl. Fig. 1C**). These abnormal nuclei did not show the typical features of apoptosis; they rather resembled the nuclear morphology of cells undergoing mitotic catastrophe (MC) (77, 78). The morphological hallmarks of MC are micro and multi-nucleation with the nuclear envelope assembled around individual clusters of mis-segregated chromosomes (78, 79). Micro and multi-nucleation were both common features of ZIKV-infected hiNPC, and lamin B1 staining revealed that the individual nuclear lobules and micronuclei were indeed surrounded by nuclear envelopes (**Fig. 3C**). ZIKV induced obvious gross nuclear abnormalities in hiNPC from 12 hpi (**Fig. 3E**), and the nuclei of infected hiNPC were globally and grossly abnormal, and DNA was largely no longer replicating, at 24 hpi (**Fig. 3F**).

ZIKV infected human neural progenitors undergo mitotic catastrophe. MC results from unscheduled mitotic entry in the presence of DNA damage or unfinished DNA replication and incomplete decatenation. As a result, chromosomes cannot be properly segregated, and pulling by the mitotic spindle results in DNA damage and chromosomal bridges, and consequent mis-segregation of chromosomes. The end results are abnormal multi-lobular nuclei. As a consequence of the resulting gross genomic defects, cells die at mitosis or at subsequent cell cycles. If ZIKV-induced nuclear abnormalities were indicative of MC, then they should be prevented by blocking mitotic entry. To test for this possibility, we used roscovitine (Rosco), which inhibits CDK1 (and other kinases), and thus prevents mitotic entry (80). ZIKV infected cells treated with DMSO vehicle showed the features of MC, as previously observed (**Fig. 1C, Fig. 2A, B**), whereas Rosco-treated infected cells, did not (**Fig. 4A**). The nuclear morphology of Rosco-treated infections was

closer to that of mock infected cells than to that of the ZIKV-infected untreated ones. Inhibiting CDK1 (and other kinases) thus prevents the abnormal nuclear morphology induced by ZIKV. Unexpectedly, no ZIKV RF were obvious in Rosco-treated cells, as evidenced by the lack of clusters of cytoplasmic NS1 signal (**Fig. 4A**, lower panel). NS1 was still expressed, and although its accumulation was delayed by some 6 hours there was about as much NS1 in the treated cells at 24 hpi as at 18 hpi in the untreated ones (**Fig. 4B**).

Inhibiting CDK1 inhibits ZIKV replication. Given the lack of obvious NS1 positive ZIKV RF (**Fig. 4A**) and delayed NS1 accumulation (**Fig. 4B**) in Rosco-treated infections, we tested the effect of Rosco on ZIKV replication. We treated the already infected cells with serial semi-logarithmic dilutions of Rosco and titrated the infectivity released to the culture medium. There was a dose response inhibition of ZIKV replication (**Fig. 4C**) with similar potency (EC_{50}, 40 μM) as against the nuclear replicating DNA viruses HSV-1, HCMV, EBV, or VZV (81-86).

We next tested viral replication in the presence of Rosco added at selected times after infection. Cells were infected with 3 PFU of ZIKV/cell. After 1 h adsorption, the inoculum was removed and monolayers were washed and overlaid with drug-free medium or medium containing 100 μM Rosco. The drug-free medium from replicate infections was replaced every 3 h with medium containing 0 or 100 μM Rosco. The infectivity released to the culture medium by Rosco- or vehicle-treated cells was sampled every 3 h from the time of compound or vehicle addition until 24 hpi. The results are expressed as virus burst from the time of Rosco addition to 24 hpi and presented as percentage of vehicle-treated controls. Addition of Rosco immediately after adsorption resulted in about 99.7% inhibition

of ZIKV replication (**Fig. 4D**). The addition of Rosco at 3-6 h allowed only for low levels of replication, about 5-6% of untreated infections. Even when Rosco was added at 9, 12 or 15 hpi, ZIKV replicated to only 12, 19 and 18% of the levels in untreated infections, respectively. Thus, Rosco inhibits ZIKV replication even when added at 15 hours after infection.

ZIKV induces cytoplasmic CDK1 accumulation. Membrane limited cytoplasmic organelles undergo rapid morphological changes in size and shape as cells enter mitosis, fragmenting and dispersing to enable their correct inheritance between the two daughter cells (reviewed in ref: (87)). Following the nuclear pore complex (hiNPC) disassembly at prophase, nuclear envelope membrane proteins are released into the mitotic endoplasmic reticulum (ER), which is remodeled from predominantly sheets in the interphase into predominantly tubules or cisternae in mitosis (88, 89). This entire process is initiated by the cytoplasmic activity of mitotic CDK1.

ZIKV induces a large remodeling of the ER to assemble cytoplasmic RF. ZIKV-remodeled ER membranes consist of mostly tubules and cisternae, globally similar to that of the mitotic ER, and Rosco, which inhibits CDK1 (and other kinases), had inhibited the formation of these ZIKV RF (**Fig. 4A)**. We therefore asked whether ZIKV might recruit CDK1 to induce ER membrane rearrangements in order to facilitate RF assembly.

CDK1 localization varies during the cell cycle. In uninfected cells, CDK1 was dispersed throughout the cytoplasm and nucleus during interphase and started to accumulate at the nuclear periphery and centrosomes at the beginning of prophase, as expected (90). Later in mitosis, CDK1 localized around condensed chromosomes (**Suppl. Fig. 3A**). In ZIKV infected cells however, there was a cytoplasmic accumulation of CDK1 (**Fig. 5A**) starting

at 3 hours after infection, independent of any mitotic changes in nuclear morphology (**Fig. 5B**). CDK1 signal was enriched around NS1, but CDK1 and NS1 signals did not colocalize and were rather intermixed (**Fig. 5A, B**).

ZIKV induces accumulation of cytoplasmic cyclin A. CDK1 activity is highly regulated at multiple levels. Binding of cyclin A or B, cellular localization of the cyclin/CDK1 holoenzymes, several activating and inhibitory phosphorylations, and binding by specific inhibitors, all regulate CDK1 activity to prevent unscheduled mitotic entry and ensure successful exit from mitosis. ZIKV infection induced MC and abnormal cytoplasmic accumulation of CDK1. We thus asked whether either of its activating cyclins had similar localization and could thus activate CDK1.

Two families of mitotic cyclins, A and B, associate with CDK1 to promote mitotic entry (reviewed in ref. (54)). CDK1 tends to associate preferentially with CycA in early G2 and with CycB later. We first evaluated CycB. In uninfected cells, CycB was first detected as a dispersed cytoplasmic signal. At early prophase, it started to accumulate at the nuclear periphery and at the centrosomes. Later, CycB localized around condensed chromosomes and to the mitotic spindle. CycB signal was lost in anaphase, in agreement with its regulated degradation initiated by the activation of the anaphase promoting complex (APC) after the spindle assembly checkpoint is satisfied (**Suppl. Fig. 3A**). CycB localization in ZIKV infected cells was unremarkable and indistinguishable from its localization in uninfected cells (**Suppl. Fig. 3B**). CycB accumulated and degraded through the cell cycle similarly in mock- or ZIKV-infected cells.

We next evaluated CycA. In mock infected hiNPC, CycA localized predominantly to the nucleus with dispersed cytoplasmic staining, as expected (90) (**Suppl. Fig. 3A**). CycA

signal was lost in late metaphase, in agreement with its known degradation initiated by APC. Starting 3h after ZIKV infection, however, infected cells started to display abnormally localized cytoplasmic CycA, often in the absence of any obvious nuclear signal (**Fig. 5C**). The number of cells showing this abnormal localization increased with time, and all ZIKV infected cells had abnormal cytoplasmic CycA at 24 hpi, when CycA was particularly enriched around NS1. Similarly to CDK1, CycA and NS1 signals were intermixed rather than colocalized (**Fig. 5D**). All ZIKV infected cells expressed detectable levels of CycA at 24 h post infection, as opposed to the expected degradation in a large subset of mock-infected cells (**Fig. 5C**). Our results thus indicate that ZIKV infection induces cytoplasmic accumulation of CycA and CDK1.

ZIKV induces unscheduled activation of CycA/CDK1. ZIKV induced accumulation of cytoplasmic CycA and CDK1, presumably to trigger ER membrane rearrangements, correlated with gross mitotic abnormalities. We thus asked whether the abnormal accumulation of CycA and CDK1 during ZIKV infection indicated active CDK1 complexes.

We evaluated the kinase activity of CDK1 or CycA immunoprecipitates from 3 to 24 hpi. CDK1 activity increased in ZIKV infected cells from the time of infection. Following an initial steady-state increase for up to 12 hpi, there was an exponential increase in CDK1 activity, reaching on average about 5-fold higher than in non-infected cells at 21 hpi (**Fig. 5E**). CDK1 kinase activity did not change much in asynchronous control cells in the 24 h, as expected (**Fig. 5E, insert**). Similarly, CycA antibody co-immunoprecipitated kinase activity was elevated in ZIKV infected cells, to about 2-fold over control cells at 21 hpi, whereas there were no major changes in non-infected cells (**Fig. 5E**). Our results indicate

that ZIKV induces unscheduled activation of cytoplasmic CycA/CDK1 activity, activation that continuously increases until 21-24 h post ZIKV infection.

We next evaluated CycA and CDK1 expression levels through 24 h of infection. CDK1 is constitutively expressed, and its level is constant during the cell cycle. CycA expression is tightly regulated and synchronized with cell cycle progression. Its accumulation begins in late G1, peaks in mid-S phase and declines in early mitosis (52, 53). In populations of unsynchronized uninfected cells, however, levels of CycA are approximately constant, as different cells progress through the cell cycle at different times. No major differences in total CycA or CDK1 accumulation in the populations of ZIKV- infected cells were observed, and their levels were as constant as expected (**Fig. 5F**). Therefore, the elevated activity of CycA/CDK1 was not related to increased expression levels.

Although the increase in CycA/CDK1 activity thus reflects the elevated levels of CyclinA/CDK1 complexes in the cytoplasm, it should also require dysfunctional checkpoint signaling when considering the abundant DNA damage in infected cells.

DNA damage-activated checkpoints are defective in ZIKV infection. As CDK1 was active in the presence of DNA damage, we tested checkpoint activation. The G2/M checkpoint inhibits CDK1 activity to prevent mitotic progression in the presence of damaged or incompletely replicated DNA. The unscheduled activation of CycA/CDK1 in the presence of DNA damage in ZIKV infection suggested dysfunctional checkpoint signaling. DNA damage activates the ATM and the ATR kinases, which in turn phosphorylate checkpoint kinases Chk1 and Chk2 to stop cell cycle progression (reviewed in (91)).

To test checkpoint signaling, we analyzed the activation of ATM, ATR, Chk1, and Chk2 with phospho-specific antibodies recognizing their activated phosphorylated forms (ATM, pS1981; ATR, pT1989; CHK1, pS345; CHK2, pT68). We UV irradiated cells at 100 J/m^2 to control for checkpoint activation. As expected, UV irradiation resulted in the accumulation of the DNA damage marker γH2AX as well as activation of the damage sensing kinases ATM and ATR and the checkpoint kinases Chk1 and Chk2, as detected by the presence of their specific phospho-forms at 1 h post irradiation (**Fig. 6**). There was also an accumulation of total γH2AX in ZIKV infected cells, most obvious at 21 and 24 hpi. Unlike in UV-treated cells however, there was no obvious ATM activation in infected cells. The background levels of ATR activation in NPC were relatively high but did not differ between infected and mock-infected cells. This basal ATR activation in NPC likely results from their innate replication stress (92). As expected from the lack of activation of ATM or ATR, there was no downstream activation of Chk1 or Chk2 in ZIKV infected hiNPC either.

In summary, ZIKV infected cells failed to activate the cell cycle checkpoints despite the presence of DNA damage, CDK1 was thus activated and triggered mitosis in the presence of DNA damage, which remained unrepaired because of the functional PNKP depletion, thus resulting in MC.

Discussion

Congenital ZIKV infections preferentially target fetal neural progenitors. Infection of these cells results in a series of neurodevelopmental abnormalities of which the most serious is microcephaly. In the present study, we show a link between ZIKV infection and the DNA

damage repair enzyme PNKP, which is itself also linked to microcephaly. PNKP mislocalized to cytoplasmic clusters co-localizing with NS1, which is a marker of ZIKV RF and a PNKP phosphatase inhibitor, A12B4C3, inhibited ZIKV replication in a dose-dependent manner. ZIKV-infected human neural progenitors accumulated DNA damage but failed to activate the DNA damage checkpoint kinases Chk1 and Chk2. Consequently, they underwent defective mitoses, producing grossly abnormal nuclear morphologies consistent with the phenotype of MC. ZIKV infection also induced cytoplasmic accumulation and activation of CycA/CDK1 complexes. CDK1 inhibition inhibited the formation of ZIKV RFs and the production of ZIKV infectivity. Unscheduled activation of CycA/CDK1 and checkpoint failure lead to premature mitotic entry of infected cells in the presence of damaged or incompletely replicated DNA, which in turn lead to MC. It remains unclear at this time why nuclear depletion or cytoplasmic accumulation of PNKP would be required during the replication cycle of ZIKV, as are the mechanisms of PNKP recruitment to the RF, or of CycA/CDK1 to their proximity. It is also unclear why PNKP would participate in the replication of a cytoplasmic RNA virus, although it has a role in the replication of some nuclear DNA viruses (93, 94). We are in the process of addressing these yet outstanding issues.

The PNKP gene (MIM605610, locus 19q13.33) was identified in 1999 (34, 35). It encodes a polynucleotide 5'-kinase 3′-phosphatase involved in DNA damage repair. PNKP consists of the N-terminal forkhead-associated domain (FHA), the phosphatase domain, and C-terminal kinase domain (95). The FHA domain binds to the single strand (SSBR) or double strand DNA breaks (DSBR) scaffold proteins XRCC1 or XRCC4, respectively (70-72, 96). PNKP is thus recruited to the sites of DNA damage to repair DNA breaks with

so-called 'dirty' 3'-phosphate (3'-PO) and 5'-hydroxyl (5'-OH) termini. Restoring canonical DNA termini by the 5'-kinase and 3'-phosphatase enzymatic activities of PNKP is essential to repair DNA breaks bearing such 'dirty' termini. PNKP deficiencies hamper single and double strand break repair (SSBR and DSBR, respectively) (44, 46, 47), increasing the frequency of spontaneous mutations and sensitizing cells to genotoxic stress (45). PNKP deficient cells accumulate DNA damage and chromosomal lesions, producing mitotic abnormalities including micronuclei and chromosomal bridges (44, 47). Some PNKP genetic variants are associated with rare (less than 50 patients worldwide) autosomal recessive neurological disorders, presenting with neurodevelopmental or neurodegenerative symptoms. The most severe of these disorders produces early onset primary microcephaly with seizures and developmental delay (MCSZ, MIM 613402), also known as developmental and epileptic encephalopathy-10, DEE10) (31, 97). Other PNKP mutations are linked to milder conditions, such as neurodegenerative ataxia with oculomotor apraxia 4 (AOA4) (98-100), late onset Charcot-Marie-Tooth disease 2B2 (CMT2B2) (101, 102), or a developmental early onset epileptic encephalopathy-12 without microcephaly (DEE12) (33). Of the 20 disease-causing single-gene patient-reported PNKP mutations with confirmed clinical diagnoses (**Suppl. Tabl. 3,** *https://www.ncbi.nlm.nih.gov/clinvar/?term=PNKP%5Bgene%5D, 2021*), 10 map to the kinase domain (aa 341-516), of which six result in MCSZ. Only four pathogenic PNKP mutations map to the phosphatase domain (aa 146-337) and all have been identified in MCSZ. Of the three pathogenic PNKP mutations in the FHA domain (aa 6-110), two are associated with MCSZ. Lastly, three mutations map to the unstructured regions, but none of them segregates with MCSZ.

It is not entirely clear how different PNKP mutations contribute to either neurodevelopmental or neurodegenerative pathologies, but recent data indicate that residual levels of phosphatase or kinase activity may play a role. In-silico genetic variant analysis (103) shows that the phosphatase domain has lower tolerability to variation. This domain has lower variant rates, higher degree of sequence conservation, lower dN/dS ratio, and more disease-propensity hotspots than the kinase domain (103). The phosphatase domain pathogenic variants were predicted to be rare and to produce more severe clinical outcomes, a model supported by studies with patient-isolated fibroblasts. Reduced phosphatase activity of PNKP mutants and inability to repair 3'-PO single stranded DNA breaks correlated with neurodevelopmental disorders (MCSZ), whereas reduced kinase activity in the context of functional phosphatase correlated with milder neurodegenerative pathologies (44).

Inhibition of PNKP phosphatase activity by the small molecule inhibitor A12B4C3 inhibited the repair of single and double stranded DNA breaks, and sensitized cancer cells to topoisomerase poison camptothecin and γ-irradiation (65, 66, 73, 74).

Here we found that the PNKP phosphatase inhibitor A12B4C3 also inhibits ZIKV replication in a dose-dependent manner (Fig. 1A), suggesting that PNKP might play an important role in ZIKV replication. However, PNKP normally localizes to the nucleus and mitochondria (69, 104) and ZIKV replicates in cytoplasmic ER-derived RF (22, 24, 25). Surprisingly, PNKP clustered in the cytoplasm in ZIKV-infected cells co-localizing with NS1, a marker of RF (**Fig. 1C, E, Suppl. Fig. 1C, D**). As ZIKV infection did not affect total PNKP levels (**Fig.1B, Suppl. Fig.1B**), PNKP re-localizes to these cytoplasmic clusters from the nucleus and possibly mitochondria. The resulting depletion of phosphorylated

nuclear PNKP (**Fig. 2B, Suppl. Fig. 2C**) likely results in functional enzyme deficiency and the consequent accumulation of unrepaired DNA breaks. A recently identified PNKP mutation in an individual with MCSZ (P101L in the FHA domain) results in a novel nuclear export signal and consequently cytoplasmic PNKP localization (Jiang et al., unpublished data). Nuclear PNKP depletion, like the one induced by ZIKV, may therefore be sufficient to induce neurodevelopmental defects and microcephaly.

Following genotoxic stress, the DNA damage-activated ATM kinase phosphorylates PNKP at Ser114 to prevent PNKP proteasomal degradation, thus allowing efficient recruitment and accumulation of PNKP at the damage sites (68, 75, 76). Although ZIKV-infected cells accumulated DNA damage (**Fig. 2A, Fig. 6, Suppl. Fig. 2A**), there were no phosphorylated PNKP foci (**Fig. 2B, Suppl. Fig. 2C**). PNKP was thus not efficiently activated at DNA damage sites. PNKP is recruited to DNA breaks by direct interaction between its FHA domain and the DDR scaffolding proteins, X-ray repair cross complementing protein 1 (XRCC1), or 4 (XRCC4) (71, 72, 96). PNKP could thus have been recruited to the viral RF by either. However, ZIKV-induced cytoplasmic PNKP localization was independent of XRCC1 or XRCC4, which both remained nuclear (**Fig. 1F**).

DNA damage, mitotic aberrations, accumulation of chromosomal abnormalities, and death of progeny cells after mitosis have all been reported in ZIKV infected cells (105-111). Based on the analysis of the abundant and grossly abnormal nuclear morphologies in ZIKV-infected neural progenitors, seen by us (**Fig. 3 B, C**) and others (105-107), we propose that infected NPC undergo MC. MC has been defined by “the nomenclature committee on cell death” as a “regulated oncosuppressive mechanism that impedes the

proliferation or survival of cells unable to complete mitosis due to extensive DNA damage, problems with mitotic machinery, or failure of mitotic checkpoints" (112). Cells undergoing MC die at mitosis, slip out of mitosis and enter senescence, or proceed to interphase and die at subsequent cell cycles (79). MC is defined morphologically by distinct nuclear changes, including micronucleation (presence of micronuclei), multinucleation (presence of multilobular nuclei surrounded by nuclear envelope) or macronucleation (two or more nuclei collapsed into one and surrounded by nuclear envelope) (78). All the above MC phenotypes were present in ZIKV-infected NPC (**Fig. 1C; 2A, B; 3B, C**) and absent when mitotic entry was inhibited (**Fig. 4A**).

Damaged DNA causes chromosome segregation failure during mitosis and subsequent defects in mitotic exit, due to abnormal, broken, linked, or entangled chromosomes. Experimental PNKP depletion produced mitotic abnormalities in cultured astrocytes (47). However, micronuclei and chromosomal bridges, indicative of chromosome segregation failure, were detected only in PNKP deleted and also irradiated cells. No chromosomal abnormalities were detected in untreated cells despite the presence of DNA damage. We and others have observed DNA damage, mitotic abnormalities (105-111) and MC during ZIKV infection in the absence of any exogenous genotoxic stress. ZIKV-induced MC would thus require abnormal mitotic entry in the presence of the damaged DNA. Here we show that ZIKV infection induced activation of cytoplasmic CycA/CDK1 (**Fig. 5E**), triggering unscheduled mitotic entry even in the presence of DNA damage, thus leading to MC. The activity of CDK1 was elevated throughout the infection and mitotic exit did not occur, as there was continuously high CDK1 activity, leading to MC.

Premature mitosis is deleterious and therefore entry into mitosis is highly regulated. DNA damage-regulated checkpoints respond to DDR signaling by arresting cells at the G2-M and G1-S transitions to allow DNA repair or induce regulated cell death or senescence if the damage is beyond repair (for detailed recent review see ref. (91)). The main signal transducers linking DNA damage responses to checkpoint effectors are the protein serine/threonine kinases ATM and ATR. Activated ATM and ATR initiate signaling to trigger the multiple pathways of DNA repair and activate the checkpoint kinases Chk1 and Chk2 to induce temporary cell cycle arrest at G1-S or G2-M. To this end, Chk1 and Chk2 inactivate the CDC25 family phosphatases, thus inhibiting mitotic cyclin/CDK1 and preventing mitotic entry (113).

Elevated CDK1 activity in the presence of DNA damage thus also indicates checkpoint failure. Indeed, ZIKV-infected cells failed to efficiently activate the checkpoint kinases Chk1 and Chk2, although they had about as much DNA damage as uninfected cells treated with UV (**Fig. 6**). Defective ATR/Chk1 checkpoint has been reported previously in ZIKV infection in human NPC (111), while the ATM/Chk2 checkpoint was reported active, but only at 48 h post infection. In our studies, MC was induced between 12-15 h after infection and most of the infected cells presented a well defined MC phenotype at 24 h, before the previously reported ATM and Chk2 activating phosphorylations. We analyzed checkpoint activation at early times, from 3 to 24 h post infection, which would be relevant for MC at 24 h. There was no activation of Chk1 or Chk2 in ZIKV infected hiNPC as compared to their levels of phosphorylation induced by UV irradiation (**Fig. 6**).

DNA damage responses, including repair mechanisms and checkpoint signaling, are not fully activated during mitosis, to prevent telomere fusion and ensure mitotic progression

in cells already committed to mitosis (114). Most cells encountering DNA damage during mitosis continue progressing into anaphase in the presence of DNA breaks (115), while the repair mechanisms are only activated in the subsequent G1 phase (116-118). The upstream DDR responses related to the detection of DNA breaks are functional and DNA lesions are marked with γH2AX (119). However, multiple mechanisms disable the downstream DDR signaling (for recent reviews see refs. (120, 121)). The high activity of Polo-like kinase 1 (Plk1) in mitosis leads to inhibition of Chk1 and Chk2 activation despite the presence of DNA damage (122, 123). In our experiments, Chk1 and Chk2 were not activated despite the presence of abundant γH2AX staining in ZIKV infected hiNPC later in the infection (**Fig. 2A, Suppl. Fig. 2A, Fig. 6**), and CDK1 was active (**Fig. 5E**), consistently with the lack of Chk1/2 activation during ongoing mitosis.

The cytoplasmic CycA localization detected in ZIKV-infected hiNPC (**Fig. 5C, D**) is not entirely unusual. CycA localizes to the cytoplasm at the S/G2 transition where it initiates the activation of Plk1 through the phosphorylation of the cytoplasmic cofactor Bora (124). Plk1 activation in late G2 sets the commitment to mitosis (125). CDK1 and CycA accumulated in the cytoplasm of ZIKV infected cells adjacent to ZIKV RF and all ZIKV-infected cells were positive for cytoplasmic CycA at 24 hours after infection (**Fig. 5C, D**). Thus, the unscheduled mitotic entry of ZIKV-infected hiNPC is likely triggered by this cytoplasmic accumulation of active CycA/CDK1 complexes.

Inhibition of CDK1 (and other kinases) with Rosco inhibited the formation of ZIKV RF (**Fig. 4A**), and the consequent production of cell-free infectious ZIKV virions (**Fig. 4C, D**). ZIKV RF are derived from modified rough ER (RER) membranes (22, 24-26). The morphology of ZIKV RF is predominantly tubular or cisternal, while the RER has predominantly sheet

morphology, with the exception of the peripheral RER membranes that form the tubular networks. The ER undergoes sheet to tubule transformation during mitosis to enable the organelle partitioning to the daughter cells during cytokinesis (88, 89). CycA is involved in the reorganization of the ER network during mitosis in the *Drosophila* embryo (126) and in nuclear envelope breakdown, an event that initiates the ER rearrangement, in HeLa cells (127). We propose that ZIKV likely induces the activation and cytoplasmic accumulation of CycA/CDK1 to induce morphological changes to the ER membranes to facilitate the formation of the viral RFs. Curiously, CDKs continue to show to play important roles in the replication of RNA viruses whose replication requires no cell cycle progression (128).

Of the 25 genes linked to human autosomal recessive primary microcephaly (MCPH), 22 encode mitotic regulators (129). Mutations in the MCPH2, encoding the centrosomal protein Wdr62 linked to MCPH, delay the mitotic progression due to spindle instability leading to spindle assembly checkpoint (SAC) activation, resulting in mitotic arrest and cell death (130). Mitotic delay in murine NPC, either by pharmacological intervention or in transgenic mouse models, results in premature differentiation or death of NPC and produces microcephaly in transgenic animals (131-133). Mitotic abnormalities in ZIKV infected cells, including supernumerary centriole, multipolar spindle and chromosomal abnormalities, have been documented previously (105-107, 134). Here, we show that ZIKV infection caused the activation of cytoplasmic CycA/CDK1 and unscheduled mitotic entry in the presence of DNA breaks, which accumulated in infected cells due to the cytoplasmic localization of PNKP, leading to grossly abnormal mitoses culminating in MC.

Previous studies have proposed several alternative molecular mechanisms underlying ZIKV-induced microcephaly. The functions of several mitosis-associated proteins, CEP152 and pericentrin (centrosomal), CENPJ (centromere) and TBK1 kinase (centrosomal) are affected during ZIKV infection, leading to mitotic defects and premature differentiation or cell death (105, 134). Microcephaly-linked RNA binding protein musashi-1 (MSI1) has been proposed as a host factor promoting ZIKV replication (135). MSI1 binding to viral RNA limited binding to its endogenous targets, thus affecting the expression of proteins playing important roles in NPC function. ZIKV infection was also shown to inhibit AKT-mTOR signaling pathway, which plays essential roles in brain development and autophagy, leading to defective neurogenesis (136). ZIKV NS4A also targets another microcephaly-related protein ANKLE-2 and thus disrupts neurogenic asymmetric cell division in neural stem cells leading to microcephaly in a drosophila model (137). Mounting evidence also supports a role for the immune responses in the fetal neuropathology of ZIKV infection (138-143). Congenital Zika virus syndrome is thus most likely a result of a combination of several mechanisms and systemic processes, which we are only beginning to understand.

Similar to defects in mitotic genes, genetic defects affecting DNA damage responses often associate with neurodevelopmental defects presenting with microcephaly (144). We propose that the functional PNKP deficiency and dysregulation of CycA/CDK1 mitotic activity during ZIKV infection of neural progenitors result in MC, contributing to the molecular mechanism underlying neurodevelopmental pathologies of congenital ZIKV infections.

References

1. Anonymous. Pan American Health Organization / World Health Organization. Zika suspected and confirmed cases reported by countries and territories in the Americas Cumulative cases, 2015-2017. Updated as of 04 January 2018. Washington, D.C.:PAHO/WHO; 2017. Accessed
2. Dick GWA, Kitchen SF, Haddow AJ. 1952. Zika Virus (I). Isolations and serological specificity. Transactions of The Royal Society of Tropical Medicine and Hygiene 46:509-520.
3. Freitas DA, Souza-Santos R, Carvalho LMA, Barros WB, Neves LM, Brasil P, Wakimoto MD. 2020. Congenital Zika syndrome: A systematic review. PLOS ONE 15:e0242367.
4. Pereira HVFS, Dos Santos SP, Amâncio APRL, De Oliveira-Szejnfeld PS, Flor EO, De Sales Tavares J, Ferreira RVB, Tovar-Moll F, De Amorim MMR, Melo A. 2020. Neurological outcomes of congenital Zika syndrome in toddlers and preschoolers: a case series. The Lancet Child & Adolescent Health 4:378-387.
5. Platt DJ, Miner JJ. 2017. Consequences of congenital Zika virus infection. Current Opinion in Virology 27:1-7.
6. Mead PS, Hills SL, Brooks JT. 2018. Zika virus as a sexually transmitted pathogen. Current Opinion in Infectious Diseases 31.
7. Foy BD, Kobylinski KC, Foy JLC, Blitvich BJ, Travassos Da Rosa A, Haddow AD, Lanciotti RS, Tesh RB. 2011. Probable Non–Vector-borne Transmission of Zika Virus, Colorado, USA. Emerging Infectious Diseases 17:880-882.
8. Sakkas H, Bozidis P, Giannakopoulos X, Sofikitis N, Papadopoulou C. 2018. An Update on Sexual Transmission of Zika Virus. Pathogens 7:66.
9. Calvet G, Aguiar RS, Melo ASO, Sampaio SA, De Filippis I, Fabri A, Araujo ESM, De Sequeira PC, De Mendonça MCL, De Oliveira L, Tschoeke DA, Schrago CG, Thompson FL, Brasil P, Dos Santos FB, Nogueira RMR, Tanuri A, De Filippis AMB. 2016. Detection and sequencing of Zika virus from amniotic fluid of fetuses with microcephaly in Brazil: a case study. The Lancet Infectious Diseases 16:653-660.
10. Rubin EJ, Greene MF, Baden LR. 2016. Zika Virus and Microcephaly. New England Journal of Medicine 374:984-985.

11. Martines RB, Bhatnagar J, De Oliveira Ramos AM, Davi HPF, Iglezias SDA, Kanamura CT, Keating MK, Hale G, Silva-Flannery L, Muehlenbachs A, Ritter J, Gary J, Rollin D, Goldsmith CS, Reagan-Steiner S, Ermias Y, Suzuki T, Luz KG, De Oliveira WK, Lanciotti R, Lambert A, Shieh W-J, Zaki SR. 2016. Pathology of congenital Zika syndrome in Brazil: a case series. The Lancet 388:898-904.
12. Oliveira Melo AS, Malinger G, Ximenes R, Szejnfeld PO, Alves Sampaio S, Bispo De Filippis AM. 2016. Zika virus intrauterine infection causes fetal brain abnormality and microcephaly: tip of the iceberg? Ultrasound in Obstetrics & Gynecology 47:6-7.
13. Brasil P, Vasconcelos Z, Kerin T, Gabaglia CR, Ribeiro IP, Bonaldo MC, Damasceno L, Pone MV, Pone S, Zin A, Tsui I, Adachi K, Pereira JP, Gaw SL, Carvalho L, Cunha DC, Guida L, Rocha M, Cherry JD, Wang L, Aliyari S, Cheng G, Foo S-S, Chen W, Jung J, Brickley E, Moreira MEL, Nielsen-Saines K. 2020. Zika virus vertical transmission in children with confirmed antenatal exposure. Nature Communications 11.
14. Ades AE, Soriano-Arandes A, Alarcon A, Bonfante F, Thorne C, Peckham CS, Giaquinto C. 2021. Vertical transmission of Zika virus and its outcomes: a Bayesian synthesis of prospective studies. The Lancet Infectious Diseases 21:537-545.
15. Christian KM, Song H, Ming GL. 2019. Pathophysiology and Mechanisms of Zika Virus Infection in the Nervous System. Annu Rev Neurosci 42:249-269.
16. Xu D, Li C, Qin C-F, Xu Z. 2019. Update on the Animal Models and Underlying Mechanisms for ZIKV-Induced Microcephaly. Annual Review of Virology 6:459-479.
17. Barkovich AJ, Dobyns WB, Guerrini R. 2015. Malformations of Cortical Development and Epilepsy. Cold Spring Harbor Perspectives in Medicine 5:a022392-a022392.
18. Wen Z, Song H, Ming GL. 2017. How does Zika virus cause microcephaly? Genes Dev 31:849-861.
19. Kuno G, Chang GJJ. 2007. Full-length sequencing and genomic characterization of Bagaza, Kedougou, and Zika viruses. Archives of Virology 152:687-696.

20. Hou W, Cruz-Cosme R, Armstrong N, Obwolo LA, Wen F, Hu W, Luo M-H, Tang Q. 2017. Molecular cloning and characterization of the genes encoding the proteins of Zika virus. Gene 628:117-128.
21. Wang A, Thurmond S, Islas L, Hui K, Hai R. 2017. Zika virus genome biology and molecular pathogenesis. Emerging Microbes & Infections 6:1-6.
22. Mohd Ropidi MI, Khazali AS, Nor Rashid N, Yusof R. 2020. Endoplasmic reticulum: a focal point of Zika virus infection. Journal of Biomedical Science 27.
23. Rossignol ED, Peters KN, Connor JH, Bullitt E. 2017. Zika virus induced cellular remodelling. Cellular Microbiology 19:e12740.
24. Caldas LA, Azevedo RC, Da Silva JL, De Souza W. 2020. Microscopy analysis of Zika virus morphogenesis in mammalian cells. Scientific Reports 10.
25. Ci Y, Liu Z-Y, Zhang N-N, Niu Y, Yang Y, Xu C, Yang W, Qin C-F, Shi L. 2020. Zika NS1–induced ER remodeling is essential for viral replication. Journal of Cell Biology 219.
26. Cortese M, Goellner S, Acosta EG, Neufeldt CJ, Oleksiuk O, Lampe M, Haselmann U, Funaya C, Schieber N, Ronchi P, Schorb M, Pruunsild P, Schwab Y, Chatel-Chaix L, Ruggieri A, Bartenschlager R. 2017. Ultrastructural Characterization of Zika Virus Replication Factories. Cell Reports 18:2113-2123.
27. Neufeldt CJ, Cortese M, Acosta EG, Bartenschlager R. 2018. Rewiring cellular networks by members of the Flaviviridae family. Nature Reviews Microbiology 16:125-142.
28. Ci Y, Shi L. 2021. Compartmentalized replication organelle of flavivirus at the ER and the factors involved. Cellular and Molecular Life Sciences doi:10.1007/s00018-021-03834-6.
29. Delfin-Riela T, Rossotti M, Alvez-Rosado R, Leizagoyen C, Gonzalez-Sapienza G. 2020. Highly Sensitive Detection of Zika Virus Nonstructural Protein 1 in Serum Samples by a Two-Site Nanobody ELISA. Biomolecules 10.
30. Flamand M, Megret FO, Mathieu M, Lepault J, Rey FLA, Deubel V. 1999. Dengue Virus Type 1 Nonstructural Glycoprotein NS1 Is Secreted from Mammalian Cells as a Soluble Hexamer in a Glycosylation-Dependent Fashion. Journal of Virology 73:6104-6110.

31. Shen J, Gilmore EC, Marshall CA, Haddadin M, Reynolds JJ, Eyaid W, Bodell A, Barry B, Gleason D, Allen K, Ganesh VS, Chang BS, Grix A, Hill RS, Topcu M, Caldecott KW, Barkovich AJ, Walsh CA. 2010. Mutations in PNKP cause microcephaly, seizures and defects in DNA repair. Nature Genetics 42:245-249.
32. Dumitrache LC, McKinnon PJ. 2017. Polynucleotide kinase-phosphatase (PNKP) mutations and neurologic disease. Mechanisms of Ageing and Development 161:121-129.
33. Poulton C, Oegema R, Heijsman D, Hoogeboom J, Schot R, Stroink H, Willemsen MA, Verheijen FW, Van De Spek P, Kremer A, Mancini GMS. 2013. Progressive cerebellar atrophy and polyneuropathy: expanding the spectrum of PNKP mutations. neurogenetics 14:43-51.
34. Karimi-Busheri F, Daly G, Robins P, Canas B, Pappin DJ, Sgouros J, Miller GG, Fakhrai H, Davis EM, Le Beau MM, Weinfeld M. 1999. Molecular characterization of a human DNA kinase. J Biol Chem 274:24187-94.
35. Jilani A, Ramotar D, Slack C, Ong C, Yang XM, Scherer SW, Lasko DD. 1999. Molecular Cloning of the Human Gene, PNKP, Encoding a Polynucleotide Kinase 3′-Phosphatase and Evidence for Its Role in Repair of DNA Strand Breaks Caused by Oxidative Damage. Journal of Biological Chemistry 274:24176-24186.
36. Weinfeld M, Mani RS, Abdou I, Aceytuno RD, Glover JNM. 2011. Tidying up loose ends: the role of polynucleotide kinase/phosphatase in DNA strand break repair. Trends in Biochemical Sciences 36:262-271.
37. Bertoncini CRA, Mene R. 1995. DNA strand breaks produced by oxidative stress in mammalian cells exhibit 3′-phosphoglycolate termini. Nucleic Acids Research 23:2995-3002.
38. Henner WD, Grunberg SM, Haseltine WA. 1982. Sites and structure of gamma radiation-induced DNA strand breaks. Journal of Biological Chemistry 257:11750-11754.
39. Yang SW, Burgin AB, Huizenga BN, Robertson CA, Yao KC, Nash HA. 1996. A eukaryotic enzyme that can disjoin dead-end covalent complexes between DNA and type I topoisomerases. Proceedings of the National Academy of Sciences 93:11534-11539.

40. Wiederhold L, Leppard JB, Kedar P, Karimi-Busheri F, Rasouli-Nia A, Weinfeld M, Tomkinson AE, Izumi T, Prasad R, Wilson SH, Mitra S, Hazra TK. 2004. AP Endonuclease-Independent DNA Base Excision Repair in Human Cells. Molecular Cell 15:209-220.
41. Coquerelle T, Bopp A, Kessler B, Hagen U. 1973. Strand Breaks and 5′ End-groups in DNA of Irradiated Thymocytes. International Journal of Radiation Biology and Related Studies in Physics, Chemistry and Medicine 24:397-404.
42. Hsiang YH, Hertzberg R, Hecht S, Liu LF. 1985. Camptothecin induces protein-linked DNA breaks via mammalian DNA topoisomerase I. Journal of Biological Chemistry 260:14873-14878.
43. Terzoudi GI, Karakosta M, Pantelias A, Hatzi VI, Karachristou I, Pantelias G. 2015. Stress induced by premature chromatin condensation triggers chromosome shattering and chromothripsis at DNA sites still replicating in micronuclei or multinucleate cells when primary nuclei enter mitosis. Mutat Res Genet Toxicol Environ Mutagen 793:185-98.
44. Kalasova I, Hailstone R, Bublitz J, Bogantes J, Hofmann W, Leal A, Hanzlikova H, Caldecott KW. 2020. Pathological mutations in PNKP trigger defects in DNA single-strand break repair but not DNA double-strand break repair. Nucleic Acids Research 48:6672-6684.
45. Rasouli-Nia A, Karimi-Busheri F, Weinfeld M. 2004. Stable down-regulation of human polynucleotide kinase enhances spontaneous mutation frequency and sensitizes cells to genotoxic agents. Proceedings of the National Academy of Sciences 101:6905-6910.
46. Reynolds JJ, Walker AK, Gilmore EC, Walsh CA, Caldecott KW. 2012. Impact of PNKP mutations associated with microcephaly, seizures and developmental delay on enzyme activity and DNA strand break repair. Nucleic Acids Research 40:6608-6619.
47. Shimada M, Dumitrache LC, Russell HR, McKinnon PJ. 2015. Polynucleotide kinase–phosphatase enables neurogenesis via multiple DNA repair pathways to maintain genome stability. The EMBO Journal 34:2465-2480.

48. Heim A, Rymarczyk B, Mayer TU. 2017. Regulation of Cell Division, p 83-116 doi:10.1007/978-3-319-46095-6_3. Springer International Publishing.
49. De Souza R, Costa Ayub L, Yip K. 2018. Mitotic Catastrophe, p 475-510, Apoptosis and Beyond doi:https://doi.org/10.1002/9781119432463.ch23.
50. Crncec A, Hochegger H. 2019. Triggering mitosis. FEBS Letters 593:2868-2888.
51. Katsuno Y, Suzuki A, Sugimura K, Okumura K, Zineldeen DH, Shimada M, Niida H, Mizuno T, Hanaoka F, Nakanishi M. 2009. Cyclin A-Cdk1 regulates the origin firing program in mammalian cells. Proceedings of the National Academy of Sciences 106:3184-3189.
52. Den Elzen N, Pines J. 2001. Cyclin a Is Destroyed in Prometaphase and Can Delay Chromosome Alignment and Anaphase. Journal of Cell Biology 153:121-136.
53. Geley S, Kramer E, Gieffers C, Gannon J, Peters J-M, Hunt T. 2001. Anaphase-Promoting Complex/Cyclosome–Dependent Proteolysis of Human Cyclin a Starts at the Beginning of Mitosis and Is Not Subject to the Spindle Assembly Checkpoint. Journal of Cell Biology 153:137-148.
54. Martínez-Alonso D, Malumbres M. 2020. Mammalian cell cycle cyclins. Seminars in Cell & Developmental Biology 107:28-35.
55. Fung T, Poon R. 2005. A roller coaster ride with the mitotic cyclins. Seminars in Cell & Developmental Biology 16:335-342.
56. Mueller PR, Coleman TR, Kumagai A, Dunphy WG. 1995. Myt1: A Membrane-Associated Inhibitory Kinase That Phosphorylates Cdc2 on Both Threonine-14 and Tyrosine-15. Science 270:86-90.
57. Kornbluth S, Sebastian B, Hunter T, Newport J. 1994. Membrane localization of the kinase which phosphorylates p34cdc2 on threonine 14. Molecular Biology of the Cell 5:273-282.
58. Liu F, Stanton JJ, Wu Z, Piwnica-Worms H. 1997. The human Myt1 kinase preferentially phosphorylates Cdc2 on threonine 14 and localizes to the endoplasmic reticulum and Golgi complex. Molecular and Cellular Biology 17:571-583.
59. Parker L, Piwnica-Worms H. 1992. Inactivation of the p34cdc2-cyclin B complex by the human WEE1 tyrosine kinase. Science 257:1955-1957.

60. Solomon MJ, Lee T, Kirschner MW. 1992. Role of phosphorylation in p34cdc2 activation: identification of an activating kinase. Molecular Biology of the Cell 3:13-27.
61. Kaldis P. 1999. The cdk-activating kinase (CAK): from yeast to mammals. Cellular and Molecular Life Sciences CMLS 55:284-296.
62. Kumagai A, Dunphy WG. 1991. The cdc25 protein controls tyrosine dephosphorylation of the cdc2 protein in a cell-free system. Cell 64:903-914.
63. Strausfeld U, Labbé JC, Fesquet D, Cavadore JC, Picard A, Sadhu K, Russell P, Dorée M. 1991. Dephosphorylation and activation of a p34cdc2/cyclin B complex in vitro by human CDC25 protein. Nature 351:242-245.
64. Gautier J, Solomon MJ, Booher RN, Bazan JF, Kirschner MW. 1991. cdc25 is a specific tyrosine phosphatase that directly activates p34cdc2. Cell 67:197-211.
65. Freschauf GK, Karimi-Busheri F, Ulaczyk-Lesanko A, Mereniuk TR, Ahrens A, Koshy JM, Rasouli-Nia A, Pasarj P, Holmes CFB, Rininsland F, Hall DG, Weinfeld M. 2009. Identification of a Small Molecule Inhibitor of the Human DNA Repair Enzyme Polynucleotide Kinase/Phosphatase. Cancer Research 69:7739-7746.
66. Freschauf GK, Mani RS, Mereniuk TR, Fanta M, Virgen CA, Dianov GL, Grassot J-M, Hall DG, Weinfeld M. 2010. Mechanism of Action of an Imidopiperidine Inhibitor of Human Polynucleotide Kinase/Phosphatase. Journal of Biological Chemistry 285:2351-2360.
67. Schneider CA, Rasband WS, Eliceiri KW. 2012. NIH Image to ImageJ: 25 years of image analysis. Nat Methods 9:671-5.
68. Parsons JL, Khoronenkova SV, Dianova, II, Ternette N, Kessler BM, Datta PK, Dianov GL. 2012. Phosphorylation of PNKP by ATM prevents its proteasomal degradation and enhances resistance to oxidative stress. Nucleic Acids Res 40:11404-15.
69. Tahbaz N, Subedi S, Weinfeld M. 2012. Role of polynucleotide kinase/phosphatase in mitochondrial DNA repair. Nucleic Acids Research 40:3484-3495.
70. Aceytuno RD, Piett CG, Havali-Shahriari Z, Edwards RA, Rey M, Ye R, Javed F, Fang S, Mani R, Weinfeld M, Hammel M, Tainer JA, Schriemer DC, Lees-Miller

SP, Glover JNM. 2017. Structural and functional characterization of the PNKP-XRCC4-LigIV DNA repair complex. Nucleic Acids Res 45:6238-6251.

71. Koch CA, Agyei R, Galicia S, Metalnikov P, O'Donnell P, Starostine A, Weinfeld M, Durocher D. 2004. Xrcc4 physically links DNA end processing by polynucleotide kinase to DNA ligation by DNA ligase IV. The EMBO Journal 23:3874-3885.

72. Della-Maria J, Hegde ML, McNeill DR, Matsumoto Y, Tsai M-S, Ellenberger T, Wilson DM, Mitra S, Tomkinson AE. 2012. The Interaction between Polynucleotide Kinase Phosphatase and the DNA Repair Protein XRCC1 Is Critical for Repair of DNA Alkylation Damage and Stable Association at DNA Damage Sites. Journal of Biological Chemistry 287:39233-39244.

73. Srivastava P, Sarma A, Chaturvedi CM. 2018. Targeting DNA repair with PNKP inhibition sensitizes radioresistant prostate cancer cells to high LET radiation. PLOS ONE 13:e0190516.

74. Zereshkian A, Leyton JV, Cai Z, Bergstrom D, Weinfeld M, Reilly RM. 2014. The human polynucleotide kinase/phosphatase (hPNKP) inhibitor A12B4C3 radiosensitizes human myeloid leukemia cells to Auger electron-emitting anti-CD123 111In-NLS-7G3 radioimmunoconjugates. Nuclear Medicine and Biology 41:377-383.

75. Zolner AE, Abdou I, Ye R, Mani RS, Fanta M, Yu Y, Douglas P, Tahbaz N, Fang S, Dobbs T, Wang C, Morrice N, Hendzel MJ, Weinfeld M, Lees-Miller SP. 2011. Phosphorylation of polynucleotide kinase/ phosphatase by DNA-dependent protein kinase and ataxia-telangiectasia mutated regulates its association with sites of DNA damage. Nucleic Acids Res 39:9224-37.

76. Segal-Raz H, Mass G, Baranes-Bachar K, Lerenthal Y, Wang SY, Chung YM, Ziv-Lehrman S, Strom CE, Helleday T, Hu MC, Chen DJ, Shiloh Y. 2011. ATM-mediated phosphorylation of polynucleotide kinase/phosphatase is required for effective DNA double-strand break repair. EMBO Rep 12:713-9.

77. Castedo M, Perfettini JL, Roumier T, Andreau K, Medema R, Kroemer G. 2004. Cell death by mitotic catastrophe: a molecular definition. Oncogene 23:2825-37.

78. Vakifahmetoglu H, Olsson M, Zhivotovsky B. 2008. Death through a tragedy: mitotic catastrophe. Cell Death & Differentiation 15:1153-1162.

79. Vitale I, Galluzzi L, Castedo M, Kroemer G. 2011. Mitotic catastrophe: a mechanism for avoiding genomic instability. Nature Reviews Molecular Cell Biology 12:385-392.
80. Zhelev N, Trifonov D, Wang S, Hassan M, El Serafi I, Mitev V. 2013. From Roscovitine to CYC202 to Seliciclib – from bench to bedside: discovery and development. BioDiscovery doi:10.7750/BioDiscovery.2013.10.1.
81. Taylor SL, Kinchington PR, Brooks A, Moffat JF. 2004. Roscovitine, a cyclin-dependent kinase inhibitor, prevents replication of varicella-zoster virus. J Virol 78:2853-62.
82. Schang LM, St Vincent MR, Lacasse JJ. 2006. Five years of progress on cyclin-dependent kinases and other cellular proteins as potential targets for antiviral drugs. Antivir Chem Chemother 17:293-320.
83. Schang LM, Phillips J, Schaffer PA. 1998. Requirement for cellular cyclin-dependent kinases in herpes simplex virus replication and transcription. J Virol 72:5626-37.
84. Sanchez V, McElroy AK, Yen J, Tamrakar S, Clark CL, Schwartz RA, Spector DH. 2004. Cyclin-dependent kinase activity is required at early times for accurate processing and accumulation of the human cytomegalovirus UL122-123 and UL37 immediate-early transcripts and at later times for virus production. J Virol 78:11219-32.
85. Kudoh A, Daikoku T, Sugaya Y, Isomura H, Fujita M, Kiyono T, Nishiyama Y, Tsurumi T. 2004. Inhibition of S-phase cyclin-dependent kinase activity blocks expression of Epstein-Barr virus immediate-early and early genes, preventing viral lytic replication. J Virol 78:104-15.
86. Gutierrez-Chamorro L, Felip E, Ezeonwumelu IJ, Margeli M, Ballana E. 2021. Cyclin-dependent Kinases as Emerging Targets for Developing Novel Antiviral Therapeutics. Trends Microbiol doi:10.1016/j.tim.2021.01.014.
87. Champion L, Linder MI, Kutay U. 2017. Cellular Reorganization during Mitotic Entry. Trends in Cell Biology 27:26-41.

88. Puhka M, Joensuu M, Vihinen H, Belevich I, Jokitalo E. 2012. Progressive sheet-to-tubule transformation is a general mechanism for endoplasmic reticulum partitioning in dividing mammalian cells. Mol Biol Cell 23:2424-32.
89. Puhka M, Vihinen H, Joensuu M, Jokitalo E. 2007. Endoplasmic reticulum remains continuous and undergoes sheet-to-tubule transformation during cell division in mammalian cells. J Cell Biol 179:895-909.
90. Baptist M, Lamy F, Gannon J, Hunt T, Dumont JE, Roger PP. 1996. Expression and subcellular localization of CDK2 and cdc2 kinases and their common partner cyclin A in thyroid epithelial cells: Comparison of cyclic AMP-dependent and -independent cell cycles. Journal of Cellular Physiology 166:256-273.
91. Lanz MC, Dibitetto D, Smolka MB. 2019. DNA damage kinase signaling: checkpoint and repair at 30 years. The EMBO Journal 38.
92. Ward IM, Chen J. 2001. Histone H2AX is phosphorylated in an ATR-dependent manner in response to replicational stress. J Biol Chem 276:47759-62.
93. Yue L, Guo S, Zhang Y, Liu L, Wang Q, Wang X, Shen D, Wang L, Sun L, Wang J, Liao Y, Li Q. 2013. The modulation of phosphatase expression impacts the proliferation efficiency of HSV-1 in infected astrocytes. PLoS One 8:e79648.
94. Yue L, Guo S, Cao X, Zhang Y, Sun L, Liu L, Yan M, Li Q. 2013. PNKP knockdown by RNA interference inhibits herpes simplex virus-1 replication in astrocytes. Virol Sin 28:345-51.
95. Bernstein NK, Williams RS, Rakovszky ML, Cui D, Green R, Karimi-Busheri F, Mani RS, Galicia S, Koch CA, Cass CE, Durocher D, Weinfeld M, Glover JNM. 2005. The Molecular Architecture of the Mammalian DNA Repair Enzyme, Polynucleotide Kinase. Molecular Cell 17:657-670.
96. Loizou JI, El-Khamisy SF, Zlatanou A, Moore DJ, Chan DW, Qin J, Sarno S, Meggio F, Pinna LA, Caldecott KW. 2004. The Protein Kinase CK2 Facilitates Repair of Chromosomal DNA Single-Strand Breaks. Cell 117:17-28.
97. Entezam M, Razipour M, Talebi S, Beiraghi Toosi M, Keramatipour M. 2019. Multi affected pedigree with congenital microcephaly: WES revealed PNKP gene mutation. Brain and Development 41:182-186.

98. Rudenskaya G, Marakhonov A, Shchagina O, Lozier E, Dadali E, Akimova I, Petrova N, Konovalov F. 2019. Ataxia with Oculomotor Apraxia Type 4 with PNKP Common “Portuguese” and Novel Mutations in Two Belarusian Families. Journal of Pediatric Genetics 08:058-062.

99. Bras J, Alonso I, Barbot C, Maria, Darwent L, Orme T, Sequeiros J, Hardy J, Coutinho P, Guerreiro R. 2015. Mutations in PNKP Cause Recessive Ataxia with Oculomotor Apraxia Type 4. The American Journal of Human Genetics 96:474-479.

100. Paucar M, Malmgren H, Taylor M, Reynolds JJ, Svenningsson P, Press R, Nordgren A. 2016. Expanding the ataxia with oculomotor apraxia type 4 phenotype. Neurology Genetics 2:e49.

101. Pedroso JL, Rocha CRR, Macedo-Souza LI, De Mario V, Marques W, Barsottini OGP, Bulle Oliveira AS, Menck CFM, Kok F. 2015. Mutation inPNKPpresenting initially as axonal Charcot-Marie-Tooth disease. Neurology Genetics 1:e30.

102. Leal A, Bogantes-Ledezma S, Ekici AB, Uebe S, Thiel CT, Sticht H, Berghoff M, Berghoff C, Morera B, Meisterernst M, Reis A. 2018. The polynucleotide kinase 3′-phosphatase gene (PNKP) is involved in Charcot-Marie-Tooth disease (CMT2B2) previously related to MED25. neurogenetics 19:215-225.

103. Bermúdez-Guzmán L, Jimenez-Huezo G, Arguedas A, Leal A. 2020. Mutational survivorship bias: The case of PNKP. PLOS ONE 15:e0237682.

104. Tsukada K, Matsumoto Y, Shimada M. 2020. Linker region is required for efficient nuclear localization of polynucleotide kinase phosphatase. PLOS ONE 15:e0239404.

105. Onorati M, Li Z, Liu F, André, Nakagawa N, Li M, Maria, Forrest, Pochareddy S, Andrew, Han W, Pletikos M, Gao T, Zhu Y, Bichsel C, Varela L, Szigeti-Buck K, Lisgo S, Zhang Y, Testen A, Gao X-B, Mlakar J, Popovic M, Flamand M, Stephen, Leonard, Anton ES, Tamas, Brett, Sestan N. 2016. Zika Virus Disrupts Phospho-TBK1 Localization and Mitosis in Human Neuroepithelial Stem Cells and Radial Glia. Cell Reports 16:2576-2592.

106. Souza BSF, Sampaio GLA, Pereira CS, Campos GS, Sardi SI, Freitas LAR, Figueira CP, Paredes BD, Nonaka CKV, Azevedo CM, Rocha VPC, Bandeira AC,

Mendez-Otero R, Dos Santos RR, Soares MBP. 2016. Zika virus infection induces mitosis abnormalities and apoptotic cell death of human neural progenitor cells. Scientific Reports 6:39775.

107. Wolf B, Diop F, Ferraris P, Wichit S, Busso C, Missé D, Gönczy P. 2017. Zika virus causes supernumerary foci with centriolar proteins and impaired spindle positioning. Open Biology 7:160231.

108. Ghouzzi VE, Bianchi FT, Molineris I, Mounce BC, Berto GE, Rak M, Lebon S, Aubry L, Tocco C, Gai M, Chiotto AM, Sgrò F, Pallavicini G, Simon-Loriere E, Passemard S, Vignuzzi M, Gressens P, Di Cunto F. 2016. ZIKA virus elicits P53 activation and genotoxic stress in human neural progenitors similar to mutations involved in severe forms of genetic microcephaly and p53. Cell Death & Disease 7:e2440-e2440.

109. Glover K, Coombs KM. 2020. ZIKV Infection Induces DNA Damage Response and Alters the Proteome of Gastrointestinal Cells. Viruses 12:771.

110. Ledur PF, Karmirian K, Pedrosa CDSG, Souza LRQ, Assis-De-Lemos G, Martins TM, Ferreira JDCCG, De Azevedo Reis GF, Silva ES, Silva D, Salerno JA, Ornelas IM, Devalle S, Madeiro Da Costa RF, Goto-Silva L, Higa LM, Melo A, Tanuri A, Chimelli L, Murata MM, Garcez PP, Filippi-Chiela EC, Galina A, Borges HL, Rehen SK. 2020. Zika virus infection leads to mitochondrial failure, oxidative stress and DNA damage in human iPSC-derived astrocytes. Scientific Reports 10.

111. Hammack C, Ogden SC, Madden JC, Medina A, Xu C, Phillips E, Son Y, Cone A, Giovinazzi S, Didier RA, Gilbert DM, Song H, Ming G, Wen Z, Brinton MA, Gunjan A, Tang H. 2019. Zika Virus Infection Induces DNA Damage Response in Human Neural Progenitors That Enhances Viral Replication. Journal of Virology 93.

112. Galluzzi L, Vitale I, Aaronson SA, Abrams JM, Adam D, Agostinis P, Alnemri ES, Altucci L, Amelio I, Andrews DW, Annicchiarico-Petruzzelli M, Antonov AV, Arama E, Baehrecke EH, Barlev NA, Bazan NG, Bernassola F, Bertrand MJM, Bianchi K, Blagosklonny MV, Blomgren K, Borner C, Boya P, Brenner C, Campanella M, Candi E, Carmona-Gutierrez D, Cecconi F, Chan FKM, Chandel NS, Cheng EH, Chipuk JE, Cidlowski JA, Ciechanover A, Cohen GM, Conrad M, Cubillos-Ruiz JR, Czabotar PE, D'Angiolella V, Dawson TM, Dawson VL, De Laurenzi V, De Maria

R, Debatin K-M, Deberardinis RJ, Deshmukh M, Di Daniele N, Di Virgilio F, Dixit VM, Dixon SJ, et al. 2018. Molecular mechanisms of cell death: recommendations of the Nomenclature Committee on Cell Death 2018. Cell Death & Differentiation 25:486-541.

113. Sadoughi F, Hallajzadeh J, Asemi Z, Mansournia MA, Alemi F, Yousefi B. 2021. Signaling pathways involved in cell cycle arrest during the DNA breaks. DNA Repair 98:103047.

114. Orthwein A, Fradet-Turcotte A, Noordermeer SM, Canny MD, Brun CM, Strecker J, Escribano-Diaz C, Durocher D. 2014. Mitosis Inhibits DNA Double-Strand Break Repair to Guard Against Telomere Fusions. Science 344:189-193.

115. Rieder CL, Cole RW. 1998. Entry into Mitosis in Vertebrate Somatic Cells Is Guarded by a Chromosome Damage Checkpoint That Reverses the Cell Cycle When Triggered during Early but Not Late Prophase. Journal of Cell Biology 142:1013-1022.

116. Pedersen RT, Kruse T, Nilsson J, Oestergaard VH, Lisby M. 2015. TopBP1 is required at mitosis to reduce transmission of DNA damage to G1 daughter cells. Journal of Cell Biology 210:565-582.

117. Williams RS, Moncalian G, Williams JS, Yamada Y, Limbo O, Shin DS, Groocock LM, Cahill D, Hitomi C, Guenther G, Moiani D, Carney JP, Russell P, Tainer JA. 2008. Mre11 Dimers Coordinate DNA End Bridging and Nuclease Processing in Double-Strand-Break Repair. Cell 135:97-109.

118. Suzuki M, Suzuki K, Kodama S, Watanabe M. 2006. Phosphorylated Histone H2AX Foci Persist on Rejoined Mitotic Chromosomes in Normal Human Diploid Cells Exposed to Ionizing Radiation. Radiation Research 165:269-276.

119. Rogakou EP, Boon C, Redon C, Bonner WM. 1999. Megabase Chromatin Domains Involved in DNA Double-Strand Breaks in Vivo. Journal of Cell Biology 146:905-916.

120. Heijink AM, Krajewska M, Van Vugt MATM. 2013. The DNA damage response during mitosis. Mutation Research/Fundamental and Molecular Mechanisms of Mutagenesis 750:45-55.

121. Bakhoum SF, Kabeche L, Compton DA, Powell SN, Bastians H. 2017. Mitotic DNA Damage Response: At the Crossroads of Structural and Numerical Cancer Chromosome Instabilities. Trends in Cancer 3:225-234.
122. Benada J, Burdova K, Lidak T, von Morgen P, Macurek L. 2015. Polo-like kinase 1 inhibits DNA damage response during mitosis. Cell Cycle 14:219-31.
123. van Vugt MA, Gardino AK, Linding R, Ostheimer GJ, Reinhardt HC, Ong SE, Tan CS, Miao H, Keezer SM, Li J, Pawson T, Lewis TA, Carr SA, Smerdon SJ, Brummelkamp TR, Yaffe MB. 2010. A mitotic phosphorylation feedback network connects Cdk1, Plk1, 53BP1, and Chk2 to inactivate the G(2)/M DNA damage checkpoint. PLoS Biol 8:e1000287.
124. Silva Cascales H, Burdova K, Middleton A, Kuzin V, Müllers E, Stoy H, Baranello L, Macurek L, Lindqvist A. 2021. Cyclin A2 localises in the cytoplasm at the S/G2 transition to activate PLK1. Life Science Alliance 4:e202000980.
125. Gheghiani L, Loew D, Lombard B, Mansfeld J, Gavet O. 2017. PLK1 Activation in Late G2 Sets Up Commitment to Mitosis. Cell Reports 19:2060-2073.
126. Bergman ZJ, McLaurin JD, Eritano AS, Johnson BM, Sims AQ, Riggs B. 2015. Spatial reorganization of the endoplasmic reticulum during mitosis relies on mitotic kinase cyclin A in the early Drosophila embryo. PLoS One 10:e0117859.
127. Gong D, Pomerening JR, Myers JW, Gustavsson C, Jones JT, Hahn AT, Meyer T, Ferrell JE. 2007. Cyclin A2 Regulates Nuclear-Envelope Breakdown and the Nuclear Accumulation of Cyclin B1. Current Biology 17:85-91.
128. Schang L. 2003. The cell cycle, cyclin-dependent kinases, and viral infections: new horizons and unexpected connections. Progress in cell cycle research 5:103-24.
129. Degrassi F, Damizia M, Lavia P. 2019. The Mitotic Apparatus and Kinetochores in Microcephaly and Neurodevelopmental Diseases. Cells 9:49.
130. Chen J-F, Zhang Y, Wilde J, Hansen KC, Lai F, Niswander L. 2014. Microcephaly disease gene Wdr62 regulates mitotic progression of embryonic neural stem cells and brain size. Nature Communications 5.
131. Mitchell-Dick A, Chalem A, Pilaz L-J, Debra. 2019. Acute Lengthening of Progenitor Mitosis Influences Progeny Fate during Cortical Development in vivo. Developmental Neuroscience 41:300-317.

132. Pilaz L-J, John, Emily, Ashley, Suzuki A, Salmon E, Debra. 2016. Prolonged Mitosis of Neural Progenitors Alters Cell Fate in the Developing Brain. Neuron 89:83-99.

133. Phan TP, Maryniak AL, Boatwright CA, Lee J, Atkins A, Tijhuis A, Spierings DC, Bazzi H, Foijer F, Jordan PW, Stracker TH, Holland AJ. 2021. Centrosome defects cause microcephaly by activating the 53BP1-USP28-TP53 mitotic surveillance pathway. The EMBO Journal 40.

134. Gabriel E, Ramani A, Karow U, Gottardo M, Natarajan K, Gooi LM, Goranci-Buzhala G, Krut O, Peters F, Nikolic M, Kuivanen S, Korhonen E, Smura T, Vapalahti O, Papantonis A, Schmidt-Chanasit J, Riparbelli M, Callaini G, Krönke M, Utermöhlen O, Gopalakrishnan J. 2017. Recent Zika Virus Isolates Induce Premature Differentiation of Neural Progenitors in Human Brain Organoids. Cell Stem Cell 20:397-406.e5.

135. Chavali PL, Stojic L, Meredith LW, Joseph N, Nahorski MS, Sanford TJ, Sweeney TR, Krishna BA, Hosmillo M, Firth AE, Bayliss R, Marcelis CL, Lindsay S, Goodfellow I, Woods CG, Gergely F. 2017. Neurodevelopmental protein Musashi-1 interacts with the Zika genome and promotes viral replication. Science 357:83-88.

136. Liang Q, Luo Z, Zeng J, Chen W, Foo S-S, Lee S-A, Ge J, Wang S, Steven, Berislav, Zhao Z, Jae. 2016. Zika Virus NS4A and NS4B Proteins Deregulate Akt-mTOR Signaling in Human Fetal Neural Stem Cells to Inhibit Neurogenesis and Induce Autophagy. Cell Stem Cell 19:663-671.

137. Link N, Chung H, Jolly A, Withers M, Tepe B, Arenkiel BR, Shah PS, Krogan NJ, Aydin H, Geckinli BB, Tos T, Isikay S, Tuysuz B, Mochida GH, Thomas AX, Clark RD, Mirzaa GM, Lupski JR, Bellen HJ. 2019. Mutations in ANKLE2, a ZIKA Virus Target, Disrupt an Asymmetric Cell Division Pathway in Drosophila Neuroblasts to Cause Microcephaly. Developmental Cell 51:713-729.e6.

138. Li C, Xu D, Ye Q, Hong S, Jiang Y, Liu X, Zhang N, Shi L, Qin C-F, Xu Z. 2016. Zika Virus Disrupts Neural Progenitor Development and Leads to Microcephaly in Mice. Cell Stem Cell 19:120-126.

139. Wu K-Y, Zuo G-L, Li X-F, Ye Q, Deng Y-Q, Huang X-Y, Cao W-C, Qin C-F, Luo Z-G. 2016. Vertical transmission of Zika virus targeting the radial glial cells affects cortex development of offspring mice. Cell Research 26:645-654.

140. Shao Q, Herrlinger S, Yang S-L, Lai F, Moore JM, Brindley MA, Chen J-F. 2016. Zika virus infection disrupts neurovascular development and results in postnatal microcephaly with brain damage. Development 143:4127-4136.

141. Lin S, Yang S, He J, Guest JD, Ma Z, Yang L, Pierce BG, Tang Q, Zhang Y-J. 2019. Zika virus NS5 protein antagonizes type I interferon production via blocking TBK1 activation. Virology 527:180-187.

142. Grant A, Sanket, Tripathi S, Balasubramaniam V, Miorin L, Sourisseau M, Megan, Mari, Matthew, Sonja, García-Sastre A. 2016. Zika Virus Targets Human STAT2 to Inhibit Type I Interferon Signaling. Cell Host & Microbe 19:882-890.

143. Dang J, Tiwari SK, Lichinchi G, Qin Y, Veena, Alexey, Tariq. 2016. Zika Virus Depletes Neural Progenitors in Human Cerebral Organoids through Activation of the Innate Immune Receptor TLR3. Cell Stem Cell 19:258-265.

144. Lee Y, Choi I, Kim J, Kim K. 2016. DNA damage to human genetic disorders with neurodevelopmental defects. Journal of Genetic Medicine 13:1-13.

Acknowledgments

These studies were funded by the NIH National Institute of Neurological Disorders and Stroke (5R21NS111416) and Canadian Institutes of Health Research (PJT168869). LMS is a BWF investigator in the pathogenesis of infectious disease. The authors acknowledge the support from the Baker Institute and the College of Veterinary Medicine, Cornell University. The authors thank Dr. Roy Golsteyn (University of Lethbridge, Canada) for his advice and insightful comments regarding mitotic catastrophe and Dr. Dennis Hall (University of Alberta, Canada) for providing the PNKP inhibitor A12B4C3.

Figure legends

Figure 1. A PNKP inhibitor inhibits ZIKV replication and PNKP relocalizes to the cytoplasm in ZIKV-infected NPC, colocalizing with NS1. (A) hiNPC or U-2 OS cells were inoculated with ZIKV (MOI=3), washed, and overlaid with media containing the

PNKP inhibitor A12B4C3 or DMSO. Culture supernatants at 24 hpi were titrated on Vero cells; results expressed as percent PFU/cell relative to DMSO-treated infections; n=2; (average +/- range). (B) hiNPC infected with ZIKV R1034 (MOI=3) or mock infected were harvested at the indicated times after infection, lysed, and analyzed by WB (whole cell lysates). Immuno-reactive bands were visualized by fluorescently labelled secondary antibodies. (C, F) hiNPC were infected with ZIKV R1034 (MOI=1), fixed 24 h later, and analyzed by IF for NS1 and PNKP (C), or NS1 and XRCC1 or XRCC4 (F). (D) Infected cells showing PNKP and NS1 co-localization were counted in 5 wide field confocal images; results are expressed as percentage of ZIKV infected cells; n=2 (average, +/- STDEV for each individual experiment). (E) hiNPC infected with ZIKV R1034 (MOI=2) were fixed at the indicated times after infection and analyzed by IF for NS1 and PNKP. Images are representative of at least 2 independent experiments; scale bars, 10μm.

Figure 2. ZIKV infected NPC accumulate DNA damage but fail to accumulate phosphorylated PNKP. hiNPC infected with ZIKV (MOI=1) were fixed at 26 hpi and analyzed by IF for NS1 and γH2AX (A) or pPNKP (B). Mock-infected cells were treated with 100 μM H_2O_2 for 1 h, washed, overlaid with fresh complete medium, fixed 1 h later, and analyzed by IF for γH2Ax (A), pPNKP (B), or both (C); scale bars - 10 μm; images are representative of 3 independent experiments.

Figure 3. ZIKV induces grossly abnormal nuclear morphologies that are consistent with the hallmarks of mitotic catastrophe in hiNPC. (A) hiNPC or U-2 OS cells were infected with ZIKV R1034, (MOI=1), fixed at 24 hpi and analyzed by IF for ZIKV NS1. Cells with obvious and gross nuclear aberrations at 24 h were counted in 5 wide field

confocal images (D). Results expressed as percentage of all cells (for mock infections) or infected cells (for ZIKV infections); n=2 (average, +/- STDEV for each individual experiment). (B) Infected hiNPC, as identified by NS1 staining at 24 hpi and counterstained with DAPI were analyzed using high magnification confocal imaging. (C) hiNPC were infected with ZIKV R1034, (MOI=1), fixed at 24 hpi and analyzed by IF for NS1 and lamin B. (E) hiNPC were infected with ZIKV R1034, (MOI=3), fixed at indicated times, and analyzed by DAPI staining and IF for NS1. (F) hiNPC infected with ZIKV R1034, (MOI=3), or mock-infected, for 24 h were metabolically labelled with EdU, fixed, and stained for EdU and NS1 (IF). Scale bars, 10 μm; images are representative of 2-4 independent experiments.

Figure 4. CDK1 inhibition inhibits mitotic catastrophe in ZIKV-infected NPC and ZIKV replication. hiNPC were infected with ZIKV R1034 (MOI=3), or mock-infected, washed, and overlaid with media containing Rosco at the indicated concentrations or vehicle (DMSO) at the time of inoculum removal (A,C) or at indicated time post infection (B,D). (A) Cells were fixed at 24 hpi and analyzed by IF; images are representatives of 2 independent experiments. (B) Cells were lysed and analyzed by Western blot; images are representative of 3 independent experiments. (C) Culture supernatants at 24 hpi were titrated on Vero cells, results are expressed as burst relative to vehicle-treated infections; n=2 (avarage +/- range). (D) ZIKV infected cells were treated with 100 μM Rosco at the indicated times after infection. Culture supernatants at the time of drug addition and at 24 hpi were titrated on Vero cells; results are expressed as burst from the time of addition relative to vehicle-treated infections; n=2 (average +/- range).

Figure 5. ZIKV infection induces unscheduled activation of cytoplasmic CycA/CDK1. hiNPC were infected with ZIKV R1034, (MOI=2), fixed at 24 hpi (A,D), or at indicated times (B,C) and analyzed by IF for NS1 and CDK1 (A,B) or CycA (C,D). Scale bars – 10 μm. (E) hiNPC were infected with ZIKV R1034, (MOI=2), or mock-infected and lysed at indicated times. CDK1 or CycA were immunoprecipitated and kinase activity was evaluated by immuno-kinase assays; fold change over mock-infected cells; inserts, mock-infected cells, fold change over T_0; n=2 (average +/- range). (F) hiNPC were infected with ZIKV R1034, (MOI=2), or mock infected, lysed at indicated times, and analyzed by Western blotting. Immuno-reactive bands were visualized by fluorescently labelled secondary antibodies. Images are representative of 3 independent experiments.

Figure 6. Neither G1/S nor G2/M DNA damage checkpoints are activated in ZIKV infected hiNPC. hiNPC were infected with ZIKV R1034 (MOI=2), or mock-infected, harvested at the indicated times, lysed, and analyzed for total and phosphorylated forms of checkpoint signaling (ATM, ATR) and effector (Chk1, Chk2) kinases by Western blot. DNA damage was induced in uninfected cells by UV irradiation (100 J/m^2). Cells were allowed to recover for 1 h prior to harvesting. Immuno reactive bands were visualized by fluorescently labelled secondary antibodies. Images are representative of 3 independent experiments.

Supplementary Figure 1. PNKP colocalization with ZIKV RF was not restricted to one cell-type or viral strain. (A) hiNPC or U-2 OS cells were seeded in 96-well plates to reach 25% confluence at 24 h after plating, when test dilutions of the PNKP inhibitor were added (T_0). Relative cell numbers were evaluated daily. Results show cell doublings

relative to T_0, n=1. (B) U-2 OS cells infected with ZIKV R1034 (MOI=3), or mock infected, were harvested at the indicated times after infection, lysed, and analyzed by WB (whole cell lysates). Immunoreactive bands were visualized by fluorescently labelled secondary antibodies. (C) Vero, U-2 OS, or HEK 293 cells grown on glass coverslips were infected with ZIKV R1034 (MOI=1), and 24 h later fixed and analyzed for PNKP and ZIKV NS1, or gE, or Flavivirus antigen (IF). (D) hiNPC grown on glass coverslips were infected with ZIKV IbH-30656 (MOI=1), and 24 h later fixed and analyzed for PNKP and NS1 (IF). Scale bars, 10 μM; images are representative of 2 independent experiments.

Supplementary Figure 2. ZIKV infected hiNPS accumulate DNA damage but do not activate nuclear PNKP. (A, C) hiNPC infected with ZIKV R1034, (MOI=2), fixed at the indicated times after infection, and analyzed by IF for NS1 (GTX133324) and γH2AX (A), or NS1 (GTX634158) and pPNKP (C). Mock-infected cells were treated with100 μM H_2O_2 for 1 h, washed, overlaid with fresh complete media, fixed after 1 h recovery and analyzed by IF for γH2Ax and pPNKP; scale bars, 10 μm. Images are representative of 2 or more independent experiments.

Supplementary Figure 3. CDK1, CycA and CycB subcellular localization in mock or ZIKV-infected hiNPC. (A) uninfected hiNPC were fixed 24 h post plating and analyzed by DAPI staining and IF for CDK1 (upper panel), CycB (middle panel) or CycA (lower panel). Cells in different cell cycle phases were identified based on nuclear DNA. I, interphase; P, prophase; PM, prometaphase; M, metaphase; A, anaphase; T, telophase. (B) hiNPC's infected with ZIKV R1034 (MOI=2) were fixed at indicated times after the

infection and analyzed by IF for NS1 and CycB. Images are representative of 2 independent experiments. Scale bars, 10 μm.

target protein	antibody / Cat No.	species / clone	dilution/amount		
			IF	WB	IP
ATM	BioRad / AHP2441	R	n/a	1:250	n/a
ATM (pSer1981)	BioRad / AHP2555	R	n/a	1:500	n/a
ATR	SCBT / sc-515173	M / C1	n/a	1:100	n/a
ATR (Thr1989)	CS / 30632S	R / D5K8W	n/a	1:200	n/a
CDK1	CS / 9116S	M / POH1	1:500	n/a	n/a
CDK1	SCBT / sc-54	M / 17	n/a	1:200	n/a
CDK1	SCBT /sc-54 AC	M / 17	n/a	n/a	10μg
Chk1	SCBT/ sc-8408	M / G4	n/a	1:200	n/a
Chk1(pSer345)	CS / 2348S	R / 133D3	1:250	n/a	n/a
Chk2	SCBT/ sc-17747	M / A11	n/a	1:100	n/a
Chk2 (pThr68)	Cell Signaling / 2661S	R	n/a	1:250	n/a
CycA2	Abcam / ab181591	R / EPR17351	1:500	n/a	n/a
CycA	SCBT / sc-239	M / BF683	n/a	1:200	n/a
CycA	SCBT /sc-239 AC	M / BF683	n/a	n/a	10μg
CycB1	CS / 12231S	R / D5C10	1:500	n/a	n/a
GAPHD	CS / 2118S	R / 14C10	n/a	1:500	n/a
GAPHD	BioRad / MCA4739	M / 6C5	n/a	1:1000	n/a
γH2Ax	MS / 05-636	M / JBW301	1:1000	1:500	n/a
γH2Ax (S139)	Abcam / ab11174	R	1:1000	1:1000	n/a
Lamin B1	Abcam / ab16048	R	1:1000	n/a	n/a
PNKP	Bethyl / A300-257A	R	1:500	n/a	n/a
PNKP	Aviva / OAAN01954	R	n/a	1:250	n/a
PNKP (pSer114/Thr118)	CS / 3522S	R	1:400	n/a	n/a
ZIKV NS1	Genetex / GTX634158	M / GT5212	1:1000	n/a	n/a
ZIKV NS1	Genetex / GTX133324	R	1:1000	1:800	n/a
ZIKV gE	BEI / NR50414	M / ZV-2	1:1000	n/a	n/a
Flavivirus group antigen	BEI / NR50327	M / D1-4G2-4-15	1:1000	n/a	n/a
XRCC1	CS / 2735S	R	1:200	n/a	n/a
XRCC4	SCBT /sc-271087	M / C4	1:100	n/a	n/a

Supplementary Table. 1. Primary antibodies. SCBT, Santa Cruz Biotechnology; CS, Cell Signalling; MS, MilliporeSigma; BEI, BEI-resources; R, rabbit; M, mouse.

secondary antibody-conjugate	Cat No.	dilution	
		IF	WB
Anti-mouse Alexa 488	A11001	1:1500	1:1000
Anti-mouse Alexa 546	A11003	1:1000	1:500
Anti-mouse Alexa 647	A21235	1:1000	1:500
Anti-mouse Alexa 680	A21057	n/a	1:1000
Anti-rabbit Alexa 488	A11008	1:1500	1:1000
Anti-rabbit Alexa 546	A11010	1:1000	1:500
Anti-rabbit Alexa 647	A21244	1:1000	1:500
Anti-rabbit Alexa 790	A11367	n/a	1:1000

Supplementary Table 2. Secondary antibody conjugates. ThermoFisher Scientific/Invitrogen

Mutation (NM_007254.4)	Protein	Condition(s)	Microcephaly (-/+)
C-terminus – aa: 517-521			
(PNKP).:c.1549_1550insTGTACTGC (p.Gln517fs)	Q517fs	AOA4	-
(PNKP):c.1549C>T (p.Gln517Ter)	Q517*	CMT2B2	-
		DEE12	-
Kinase domain – aa: 341-516			
(PNKP):c.1386+49_1387-33del	del/fs	DEE12	-
		MCSZ (DEE10)	**+**
(PNKP):c.1322_1323insAGCCG (p.Gly442fs)	G442fs	AOA4	-
(PNKP):c.1317_1321dup (p.Ala441fs)	A441fs	DEE12	-
(PNKP):c.1295_1298+6del	del/fs	AOA1	-
		DEE12	-
		MCSZ (DEE10)	**+**
(PNKP):c.1253_1269dup (p.Thr424fs)	T424fs	AOA4	-
		DEE12	-
		MCSZ (DEE10)	**+**
(PNKP):c.1261_1262ins (p.Ile421fs)	I421fs	**MCSZ (DEE10)**	**+**
(PNKP):c.1251_1252ins (p.Arg418fs)	R418fs	**MCSZ (DEE10)**	**+**
(PNKP):c.1227_1228del (p.Cys409_Glu410delinsTer)	microsatellite variant	AOA4	-
			-
(PNKP):c.1221_1223del (p.Thr408del)	T408del	CMT2B2	-
		DEE12	-
		AOA4	-
		MCSZ (DEE10)	**+**
(PNKP):c.1123G>T (p.Gly375Trp)	G375W	AOA4	
		DEE12	-
Phosphatase domain – aa: 146-337			
(PNKP):c.976G>A (p.Glu326Lys)	E326K	**MCSZ (DEE10)**	**+**
(PNKP):c.829dup (p.Thr277fs)	T277fs	**MCSZ (DEE10)**	**+**
(PNKP):c.636+1G>T	SNV/splice donor	**MCSZ (DEE10)**	**+**
		CMT2B2	-
		DEE12	-
(PNKP):c.526C>T (p.Leu176Phe)	L176F	**MCSZ (DEE10)**	**+**
Unstructured linker region – aa: 111-145			
(PNKP):c.363dup (p.Thr122fs)	T122fs	DEE12	-
Fork Head Associated domain – aa: 6-110			
(PNKP):c.286G>C (p.Val96Leu)	V96L	**MCSZ (DEE10)**	**+**
(PNKP):c.148C>G (p.Gln50Glu)	Q50E	AOA4	-
(PNKP):c.103A>G (p.Arg35Gly)	R35G	**MCSZ (DEE10)**	**+**

Supplementary Table 3. Clinical spectrum of pathological PNKP mutations. Modified from PNKP[gene]-ClinVar-NCBI (https://www.ncbi.nlm.nih.gov/clinvar/?term=PNKP%5Bgene%5D). Filtered by single gene pathogenic mutations found in patients with PNKP-associated disorders with identified clinical outcomes. **fs**, frameshift; **del**, deletion; *****, STOP codon; **SNV**, single nucleotide variant; **AOA4**, Ataxia-Oculomotor Apraxia 4; **AOA1**, Ataxia-Oculomotor Apraxia 1; **CMT2B2**, Charcot-Marie-Tooth Disease Type 2B2; **DEE12**, Developmental and Epileptic Encephalopathy 12 (seizures without microcephaly); **DEE10**, Developmental and Epileptic Encephalopathy 10, also known as **MCSZ** - Microcephaly, Seizures, and Developmental Delay.

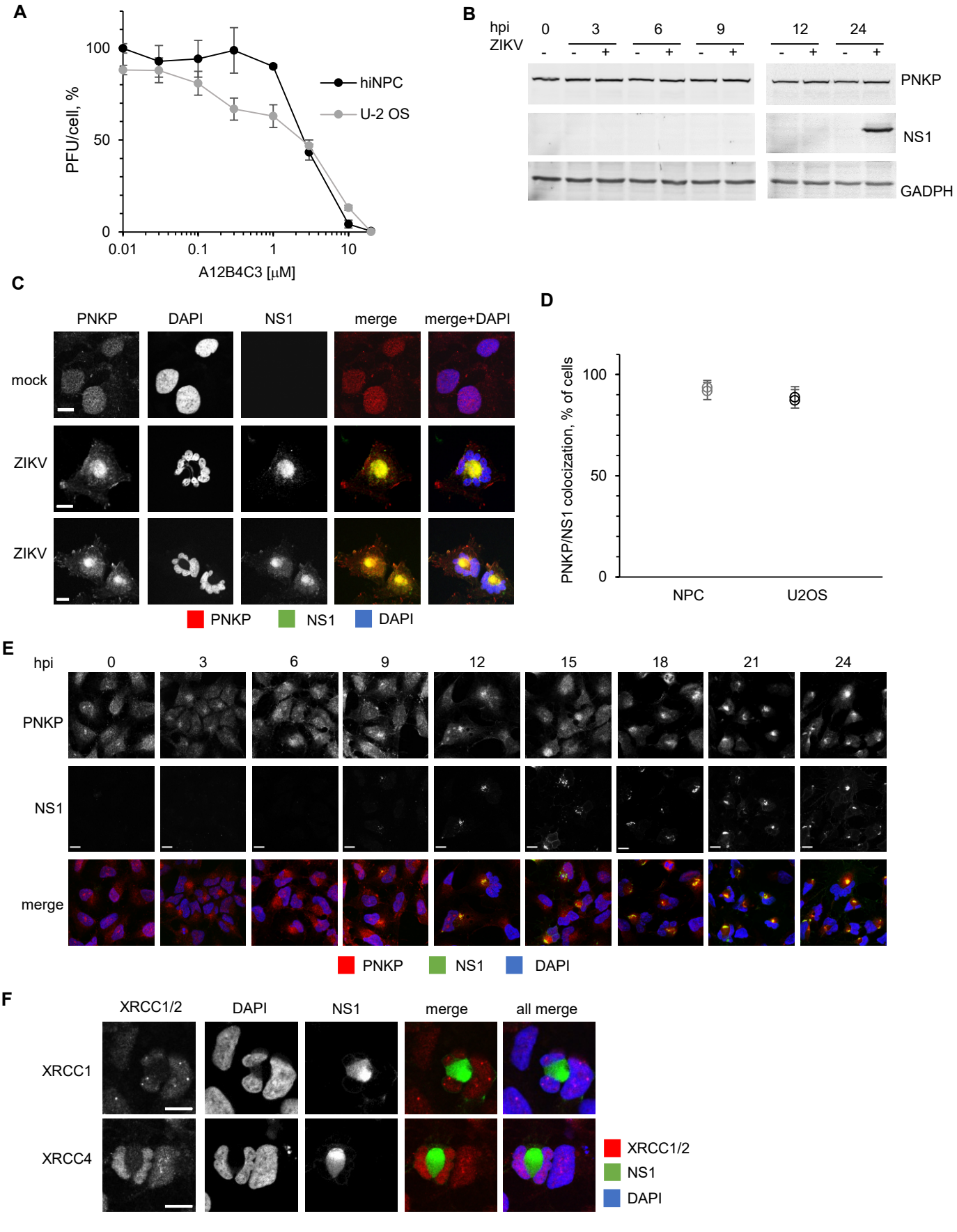
A
100
50
0
PFU/cell, %
0.01
0.1
1
10
A12B4C3 [μM]
hiNPC
U-2 OS
B
hpi
ZIKV
0
3
6
9
12
24
PNKP
NS1
GADPH
C
PNKP
DAPI
NS1
merge
merge+DAPI
mock
ZIKV
ZIKV
PNKP
NS1
DAPI
D
PNKP/NS1 colocization, % of cells
100
50
0
NPC
U2OS
E
hpi
0
3
6
9
12
15
18
21
24
PNKP
NS1
merge
PNKP
NS1
DAPI
F
XRCC1/2
DAPI
NS1
merge
all merge
XRCC1
XRCC4
XRCC1/2
NS1
DAPI

Figure 1. A PNKP inhibitor inhibits ZIKV replication and PNKP relocalizes to the cytoplasm in ZIKV-infected NPC, colocalizing with NS1. (A) ihNPC or U2OS were inoculated with ZIKV (MOI=3), washed, and overlaid with media containing the PNKP inhibitor A12B4C3A or DMSO. Culture supernatants at 24 hpi were titrated on Vero cells; results expressed as percent PFU/cell relative to DMSO-treated infections; n=2; (average +/- range). (B) ihNPC infected with ZIKV R1034 (MOI=3) or mock infected were harvested at the indicated times after infection, lysed, and analyzed by WB (whole cell lysates). Immuno-reactive bands were visualized by fluorescently labelled secondary antibodies. (C, F) ihNPC were infected with ZIKV R1034 (MOI=1), fixed 24h later, and analyzed by IF for NS1 and PNKP (C), or NS1 and XRCC1 or XRCC4 (F). (D) Infected cells showing PNKP and NS1 co-localization were counted in 5 wide field confocal images; results of expressed as percentage of ZIKV infected cells; n=2 (average, +/- STDEV for each individual experiment). (E) hiNPC infected with ZIKV R1034 (MOI=2) were fixed at the indicated times after infection and analyzed by IF for NS1 and PNKP. Images representative of at least 2 independent experiments; scale bars, 10μm.

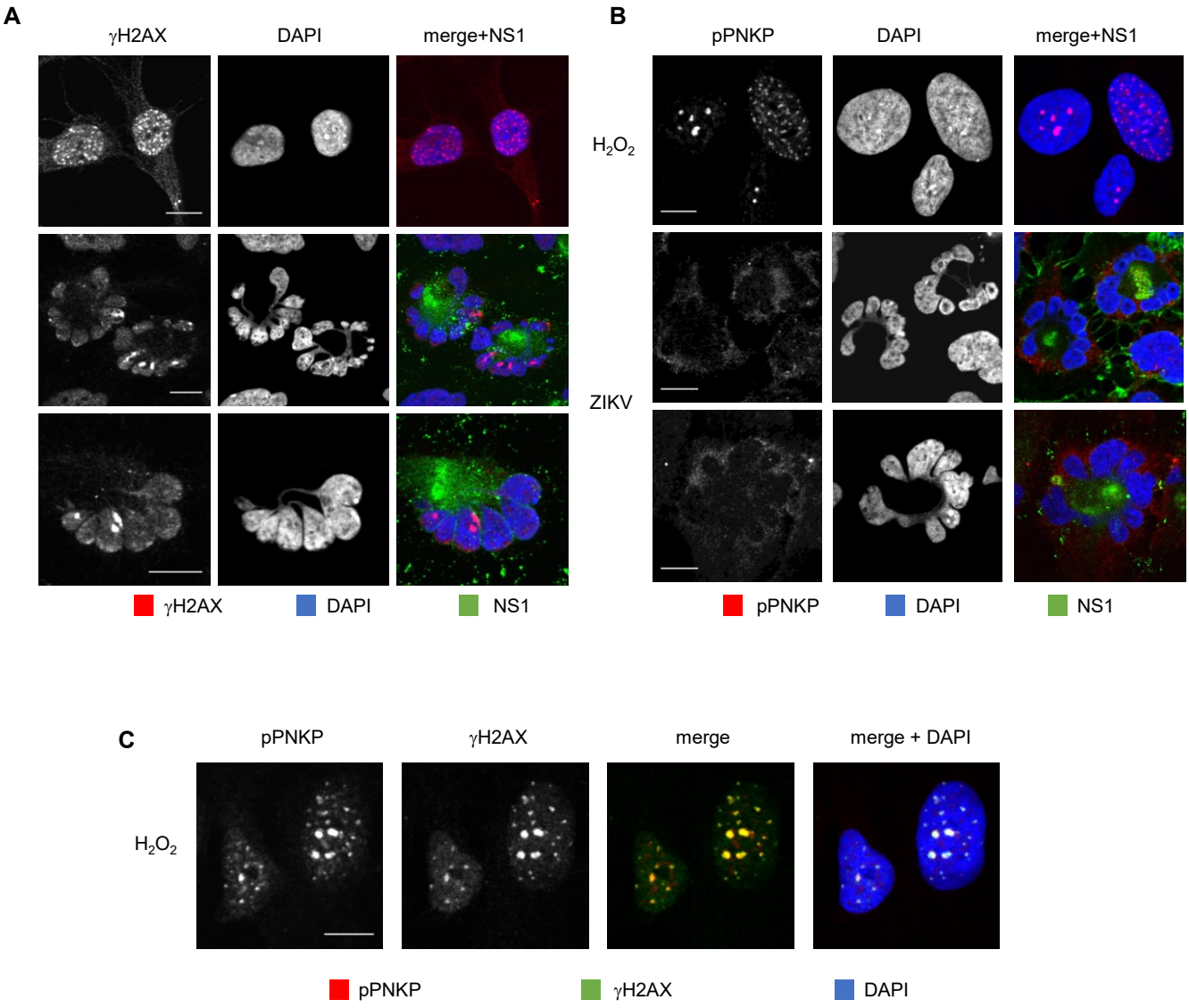

Figure 2. ZIKV infected NPC accumulate DNA damage but fail to accumulate phosphorylated PNKP. hiNPC infected with ZIKV (MOI=1) were fixed at 26 hpi and analyzed by IF for NS1 and γH2AX (A) or pPNKP (B). Mock-infected cells were treated with 100 μM H_2O_2 for 1h, washed, overlaid with fresh complete medium, fixed 1 h later, and analyzed by IF for γH2Ax (A), pPNKP (B), or both (C); scale bars - 10 μm; images representative of 3 independent experiments.

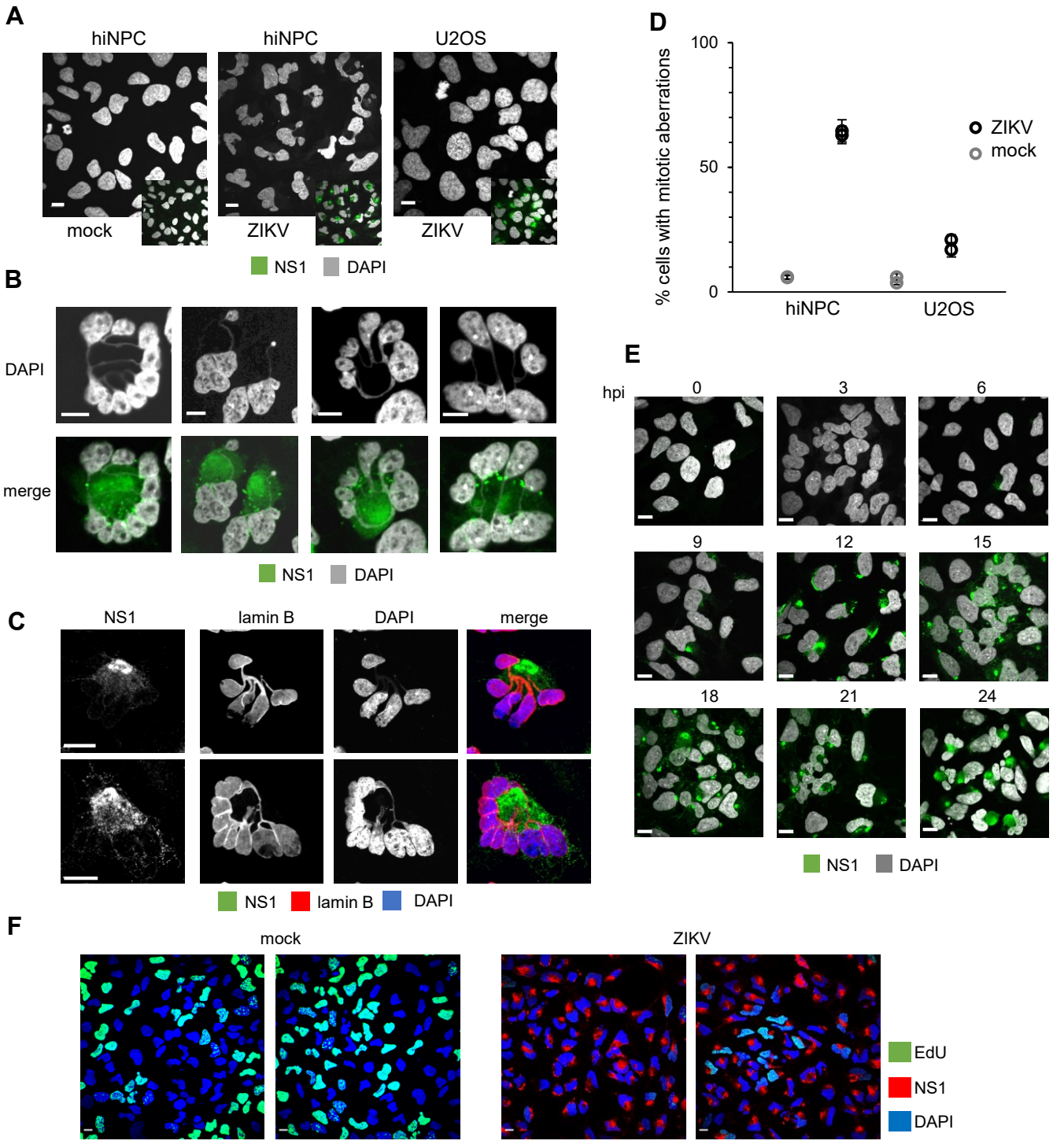

Figure 3. ZIKV induces grossly abnormal nuclear morphologies which are consistent with the hallmarks of mitotic catastrophe in hiNPC. (A) hiNPC or U2OS were infected with ZIKV R1034, (MOI=1), fixed at 24 hpi and analyzed by IF for ZIKV NS1. Cells with obvious and gross nuclear aberrations at 24 h were counted in 5 wide field confocal images (D). Results expressed as percentage of all cells (for mock infections) or infected cells (for ZIKV infections); n=2 (average, +/- STDEV for each individual experiment). (B) Infected hiNPC, as identified by NS1 staining at 24 hpi and counterstained with DAPI were analyzed using high magnification confocal imaging. (C) hiNPC were infected with ZIKV R1034, (MOI=1), fixed at 24 hpi and analyzed by IF for NS1 and lamin B. (E) hiNPC were infected with ZIKV R1034, (MOI=3), fixed at indicated times, and analyzed by DAPI staining and IF for NS1. (F) hiNPC were infected with ZIKV R1034, (MOI=3), or mock-infected, for 24 h were metabolically labelled with EdU, fixed, and stained for EdU and NS1 (IF). Scale bars, 10 μm; images representative of 2-4 independent experiments.

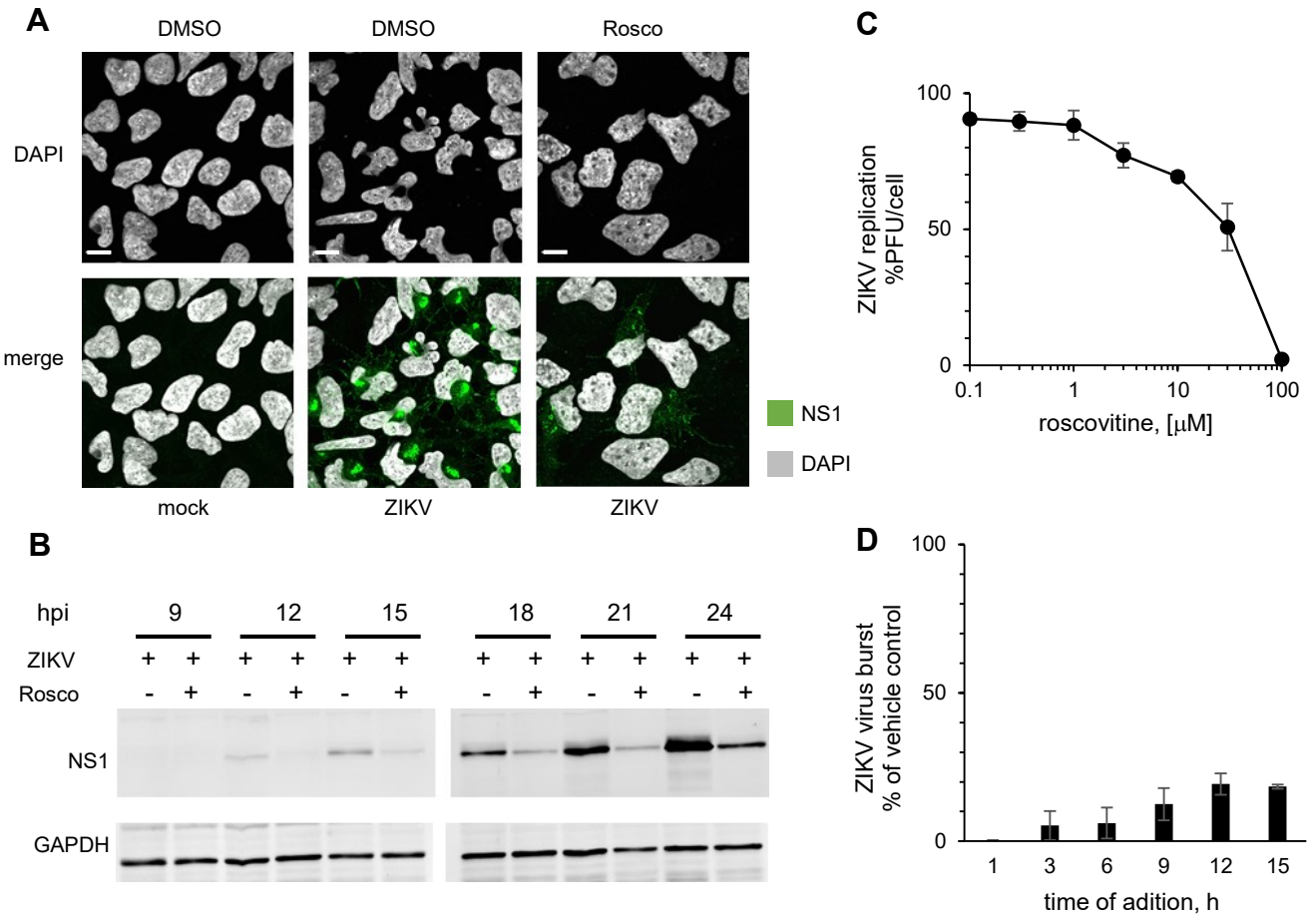

Figure 4. CDK1 inhibition inhibits mitotic catastrophe in ZIKV-infected NPC and ZIKV replication. hiNPC were infected with ZIKV R1034 (MOI=3), or mock-infected, washed, and overlaid with media containing Rosco at the indicated concentrations or vehicle (DMSO) at the time of inoculum removal (A,C) or at indicated time post infection (B,D). (A) Cells were fixed at 24 hpi and analyzed by IF; images representatives of 2 independent experiments. (B) Cells were lysed and analyzed by Western blot; images are representative of 3 independent experiments. (C) Culture supernatants at 24 hpi were titrated on Vero cells, results are expressed as burst relative to vehicle-treated infections; n=2 (avarage +/- range). (D) ZIKV infected cells were treated with 100 μM Rosco at the indicated times after infection. Culture supernatants at the time of drug addition and at 24 hpi were titrated on Vero cells; results expressed as burst from the time of addition relative to vehicle-treated infections; n=2 (average +/- range).

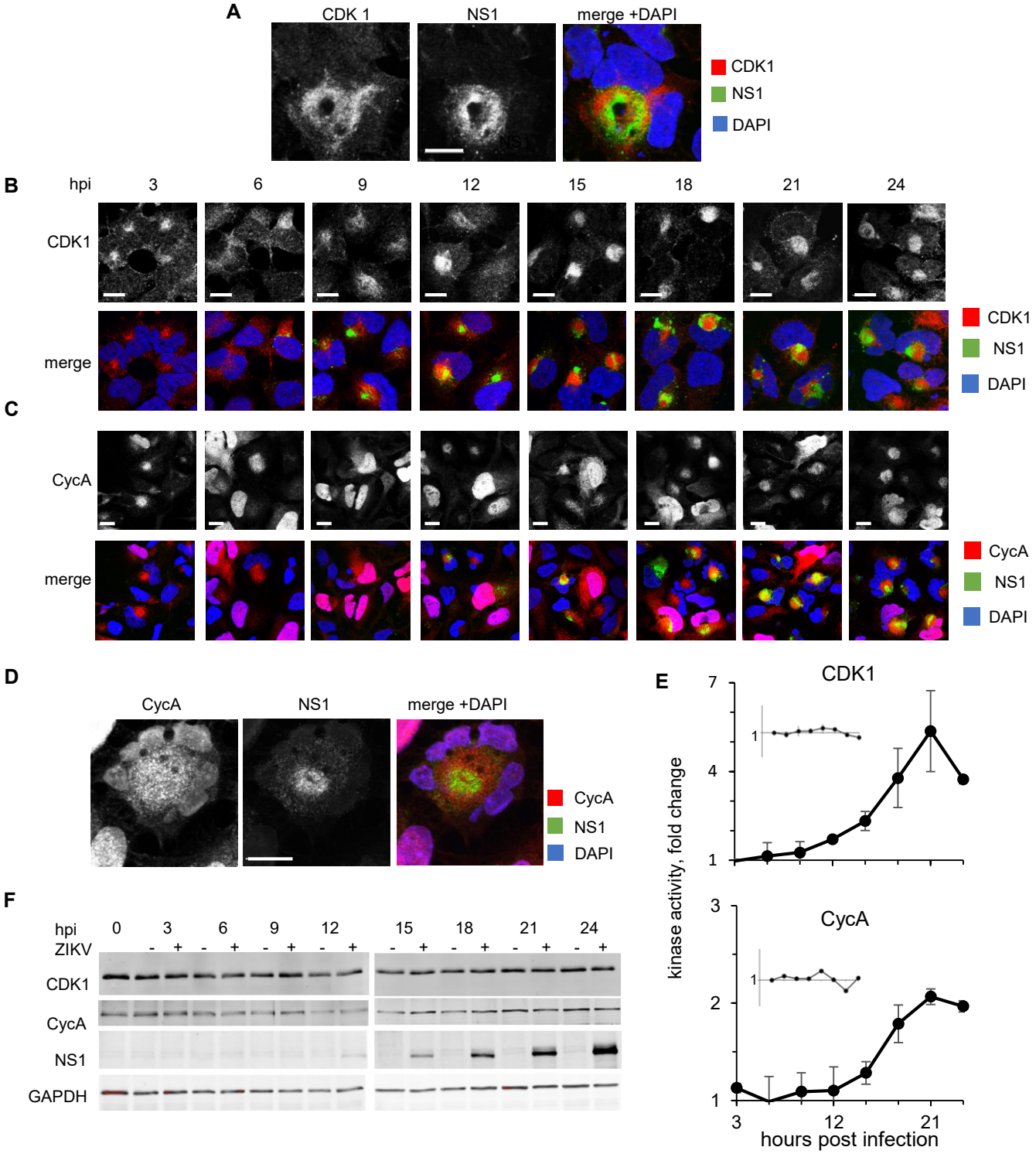

Figure 5. ZIKV infection induces unscheduled activation of cytoplasmic CycA/CDK1. hiNPC were infected with ZIKV R1034, (MOI=2), fixed at 24hpi (A,D), or at indicated times (B,C) and analyzed by IF for NS1 and CDK1 (A,B) or CycA (C,D). Scale bars - 10μm. (E) hiNPC were infected with ZIKV R1034, (MOI=2), or mock-infected and lysed at indicated times. CDK1 or CycA were immunoprecipitated and kinase activity was evaluated by immuno-kinase assays; fold change over mock-infected cells; inserts, mock-infected cells, fold change over T_0; n=2 (average +/- range). (F) hiNPC were infected with ZIKV R1034, (MOI=2), or mock infected, lysed at indicated times, and analyzed by Western blotting. Immuno-reactive bands were visualized by fluorescently labelled secondary antibodies. Images representative of 3 independent experiments.

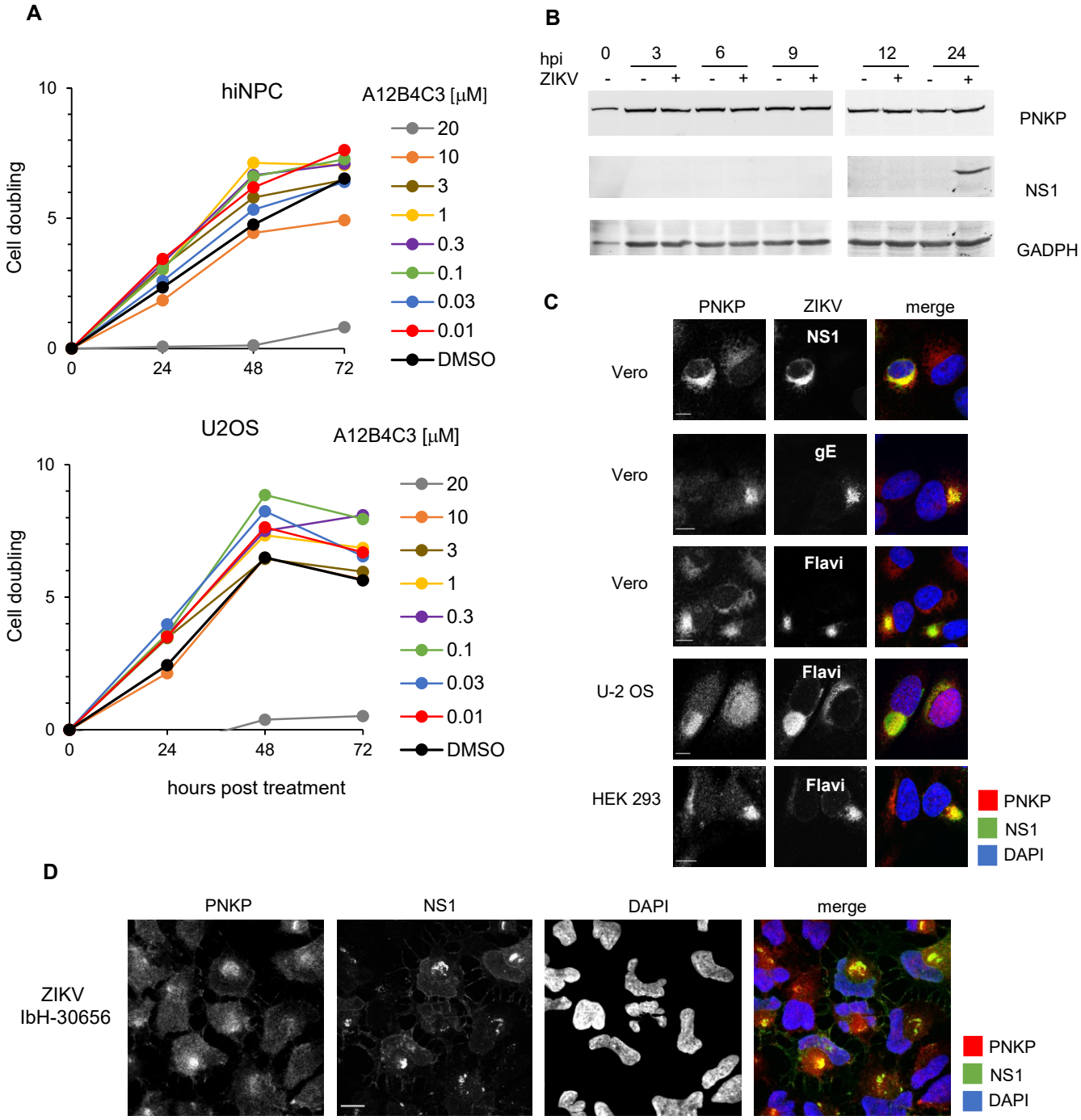

Supplementary Figure 1. PNKP colocalization with ZIKV RF was not restricted to one cell-type or viral strain. (A) ihNPC or U-2 OS cells were seeded in 96-well plates to reach 25% confluence at 24 h after plating, when test dilutions of the PNKP inhibitor were added (T_0). Relative cell numbers were evaluated daily. Results show cell doublings relative to T_0, n=1. (B) U-2 OS cells infected with ZIKV R1034 (MOI=3), or mock infected, were harvested at the indicated times after infection, lysed, and analyzed by WB (whole cell lysates). Immunoreactive bands were visualized by fluorescently labelled secondary antibodies. (C) Vero, U-2 OS, or HEK 293 cells grown on glass coverslips were infected with ZIKV R1034 (MOI=1), 24 h later cells were fixed and analyzed for PNKP and ZIKV NS1, or gE, or Flavivirus antigen (IF). (D) hiNPC grown on glass coverslips were infected with ZIKV IbH-30656 (MOI=1), 24 h later cells were fixed and analyzed for PNKP and NS1 (IF). Scale bars, 10μM; images representative of 2 independent experiments.

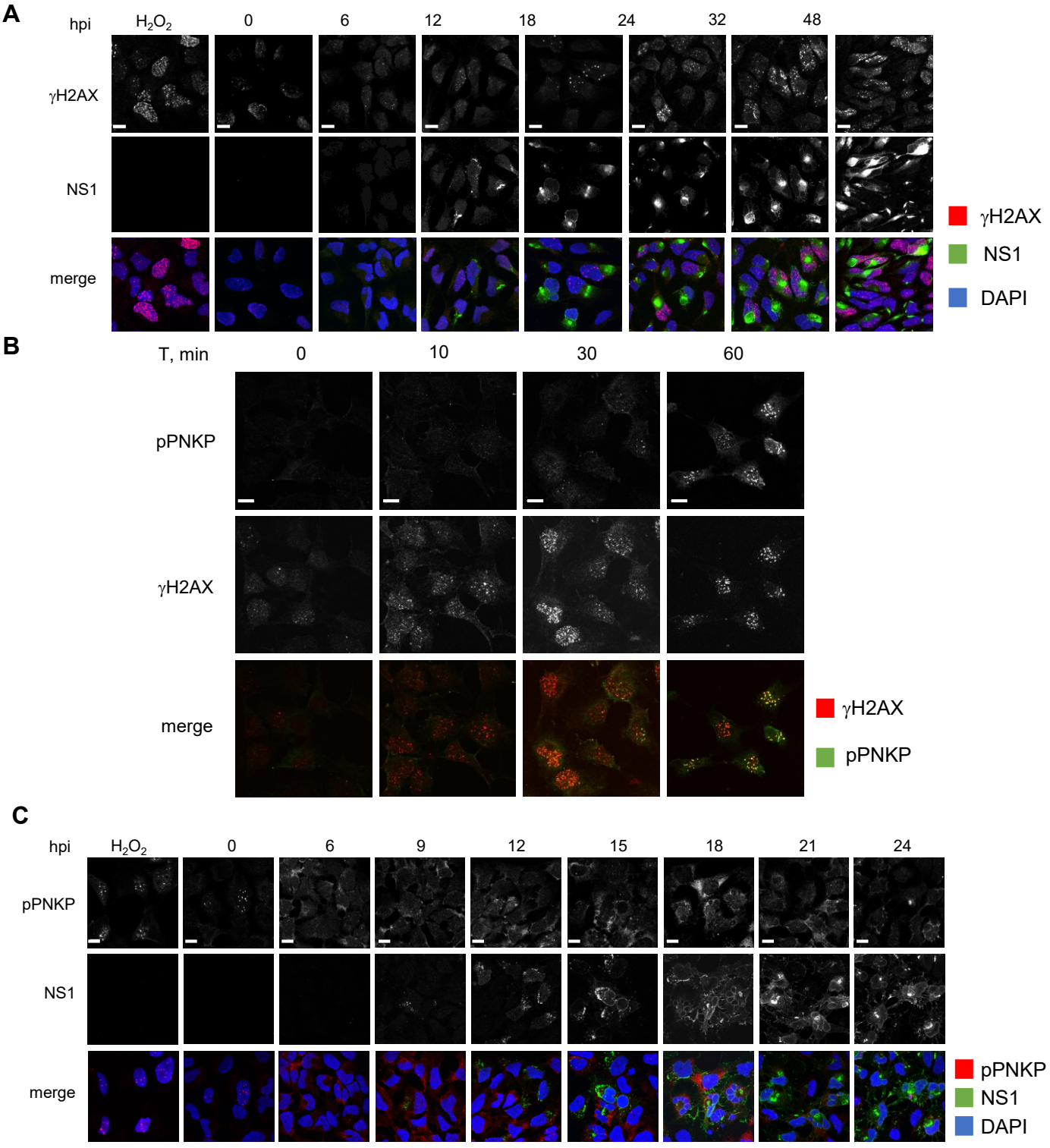

Supplementary Figure 2. ZIKV infected hiNPS accumulate DNA damage but do not activate nuclear PNKP. (A, C) hiNPC infected with ZIKV R1034, (MOI=2), fixed at the indicated times after infection, and analyzed by IF for NS1 (GTX133324) and γH2AX (A), or NS1 (GTX634158) and pPNKP (C). Mock-infected cells were treated with100μM H_2O_2 for 1h, washed, overlaid with fresh complete media, fixed after 1h recovery and analyzed by IF for γH2Ax and pPNKP; scale bars, 10μm. Images representative of 2 or more independent experiments.

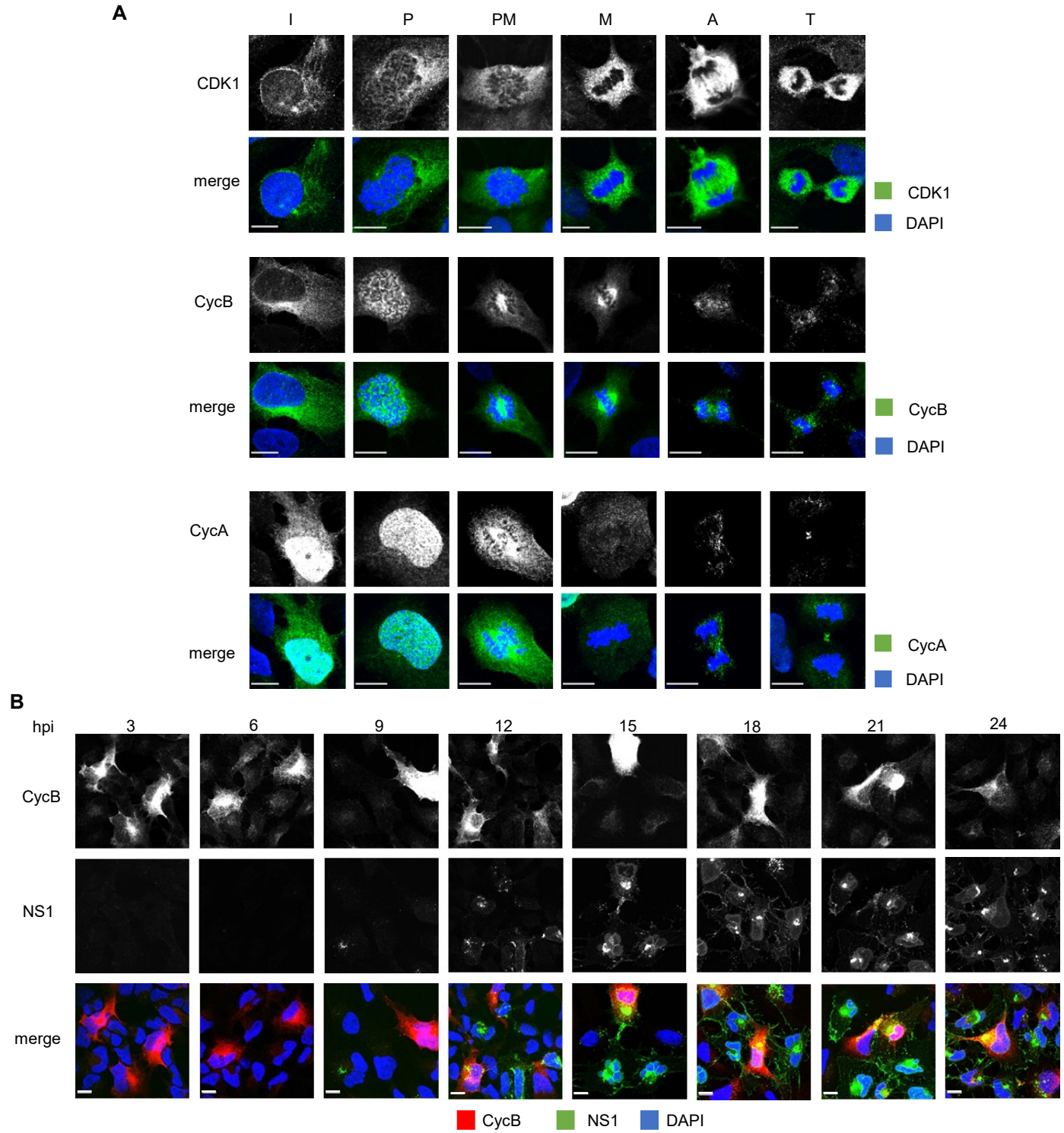

Supplementary Figure 3. CDK1, CycA and CycB subcellular localization in mock or ZIKV-infected hiNPC. (A) uninfected hiNPC were fixed 24 hours post plating and analyzed by DAPI staining and IF for CDK1 (upper panel), CycB (middle panel) or CycA (lower panel). Cells in different cell cycle phases were identified based on nuclear DNA. I, interphase; P, prophase; PM, prometaphase; M, metaphase; A, anaphase; T, telophase. (B) hiNPC's infected with ZIKV R1034 (MOI=2) were fixed at indicated times after the infection and analyzed by IF for NS1 and CycB. Images representative of 2 independent experiments. Scale bars, 10 μm.